


# Dopamine induces soluble $\alpha$ -synuclein oligomers and nigrostriatal degeneration

Danielle E Mor<sup>1</sup>, Elpida Tsika<sup>2</sup>, Joseph R Mazzulli<sup>3</sup>, Neal S Gould<sup>4</sup>, Hanna Kim<sup>5</sup>, Malcolm J Daniels<sup>6</sup>, Shachee Doshi<sup>1</sup>, Preetika Gupta<sup>1</sup>, Jennifer L Grossman<sup>7</sup>, Victor X Tan<sup>8</sup>, Robert G Kalb<sup>1,4</sup>, Kim A Caldwell<sup>5</sup>, Guy A Caldwell<sup>5</sup>, John H Wolfe<sup>1,4,9</sup> & Harry Ischiropoulos<sup>1,4,6</sup> 

Parkinson's disease (PD) is defined by the loss of dopaminergic neurons in the substantia nigra and the formation of Lewy body inclusions containing aggregated  $\alpha$ -synuclein. Efforts to explain dopamine neuron vulnerability are hindered by the lack of dopaminergic cell death in  $\alpha$ -synuclein transgenic mice. To address this, we manipulated both dopamine levels and  $\alpha$ -synuclein expression. Nigraly targeted expression of mutant tyrosine hydroxylase with enhanced catalytic activity increased dopamine levels without damaging neurons in non-transgenic mice. In contrast, raising dopamine levels in mice expressing human A53T mutant  $\alpha$ -synuclein induced progressive nigrostriatal degeneration and reduced locomotion. Dopamine elevation in A53T mice increased levels of potentially toxic  $\alpha$ -synuclein oligomers, resulting in conformationally and functionally modified species. Moreover, in genetically tractable *Caenorhabditis elegans* models, expression of  $\alpha$ -synuclein mutated at the site of interaction with dopamine prevented dopamine-induced toxicity. These data suggest that a unique mechanism links two cardinal features of PD: dopaminergic cell death and  $\alpha$ -synuclein aggregation.

PD is a debilitating neurodegenerative disorder that is principally defined by the motor symptoms of resting tremor, rigidity and bradykinesia. These symptoms occur primarily because of the progressive loss of dopaminergic neurons in the substantia nigra pars compacta (SN), which depletes dopamine at nigrostriatal synapses<sup>1</sup>. A long-standing hypothesis to explain the vulnerability of this cell population states that dopamine induces neuronal injury via oxidative stress. The enzyme- or metal-catalyzed oxidation of dopamine generates electron-deficient quinones and reactive oxygen species that can induce cellular dysfunction<sup>2,3</sup>. The SN in PD patients is reported to harbor oxidatively modified proteins, lipids and nucleic acids<sup>4–6</sup>. Efforts to study the effects of dysregulated dopamine in animal models have included ectopic dopamine administration and increased cytosolic dopamine by suppression of vesicular monoamine transporter (VMAT2) expression<sup>7–9</sup>.

More recently,  $\alpha$ -synuclein has emerged as a critical player in PD pathogenesis. Disturbances in  $\alpha$ -synuclein protein folding or expression level, that is, through mutations or extra copies of the gene that encodes it, SNCA, are known causes of PD<sup>10–17</sup>. In both familial and sporadic cases, aggregated  $\alpha$ -synuclein is present in Lewy bodies and Lewy neurites, which are the hallmark pathological lesions of the disease<sup>18,19</sup>.  $\alpha$ -Synuclein is a small, highly conserved protein (140 residues) that is abundantly expressed in the nervous system

primarily at presynaptic terminals<sup>20</sup>. The precise physiological functions of  $\alpha$ -synuclein remain unclear, although it is thought to have diverse roles in synaptic maintenance and plasticity, neurotransmitter release and homeostasis, and the regulation of synaptic vesicle pools<sup>21–23</sup>. In disease,  $\alpha$ -synuclein assembles into  $\beta$ -sheet-rich amyloid-like fibrils, generating several intermediate oligomeric species of unknown toxicity<sup>24</sup>.

Notably,  $\alpha$ -synuclein oligomers are kinetically stabilized by oxidized dopamine and other catecholamines *in vitro*<sup>24,25</sup>, providing a possible link between dopamine- and  $\alpha$ -synuclein-mediated toxicities. Extensive evidence from cultured cells and cell-free systems indicates that dopamine potently and substoichiometrically inhibits the fibrillization of  $\alpha$ -synuclein, resulting in the kinetic arrest of soluble oligomer species. Dopamine oxidation is required for oligomer stabilization, suggesting that  $\alpha$ -synuclein interacts with dopamine-quinone and/or other oxidation products. The interaction is non-covalent, reversible and dependent on residues E<sub>83</sub> and the Y<sub>125</sub>EMPS<sub>129</sub> motif in the C terminus of  $\alpha$ -synuclein<sup>24–28</sup>. The toxicity of these oligomers is largely unexplored, although *in vitro* dopamine-incubated  $\alpha$ -synuclein is reported to interfere with and resist degradation by chaperone-mediated autophagy<sup>29</sup> and to inhibit SNARE complex formation and neurotransmitter release<sup>30</sup>. It is unknown whether dopamine is able to modify  $\alpha$ -synuclein oligomerization *in vivo* and whether the

<sup>1</sup>Neuroscience Graduate Group, Perelman School of Medicine, University of Pennsylvania, Philadelphia, Pennsylvania, USA. <sup>2</sup>AC Immune SA, École Polytechnique fédérale de Lausanne Innovation Park, Lausanne, Switzerland. <sup>3</sup>Department of Neurology, Feinberg School of Medicine, Northwestern University, Chicago, Illinois, USA. <sup>4</sup>Children's Hospital of Philadelphia Research Institute, Philadelphia, Pennsylvania, USA. <sup>5</sup>Department of Biological Sciences, The University of Alabama, Tuscaloosa, Alabama, USA. <sup>6</sup>Pharmacology Graduate Group, Perelman School of Medicine, University of Pennsylvania, Philadelphia, Pennsylvania, USA. <sup>7</sup>State University of New York Downstate College of Medicine, Brooklyn, New York, USA. <sup>8</sup>College of Arts and Sciences, University of Pennsylvania, Philadelphia, Pennsylvania, USA. <sup>9</sup>W.F. Goodman Center for Comparative Medical Genetics, School of Veterinary Medicine, University of Pennsylvania, Philadelphia, Pennsylvania, USA. Correspondence should be addressed to H.I. (ischirop@mail.med.upenn.edu).

Received 8 March; accepted 22 August; published online 18 September 2017; doi:10.1038/nn.4641

resultant species are capable of driving neurodegeneration. These are the critical questions we sought to answer.

## RESULTS

### Expression of TH-RREE elevates dopamine levels and causes hyperactivity in NonTg mice

To increase dopamine levels *in vivo*, we used a lentiviral vector containing the TH gene encoding human tyrosine hydroxylase (TH). TH is the rate-limiting enzyme in dopamine biosynthesis converting tyrosine to L-DOPA, which is then metabolized by aromatic amino acid decarboxylase to generate dopamine. A mutated TH enzyme that has R<sub>37</sub>R<sub>38</sub> replaced with E<sub>37</sub>E<sub>38</sub> (TH-RREE) is insensitive to feedback inhibition by dopamine and can be used to achieve increased catalytic activity of TH<sup>26,27,31</sup>. We first tested the function of the vector on human neuroblastoma SH-SY5Y cells. This cell line has undetectable levels of endogenous TH, despite the expression of other enzymes required for synthesis and processing of dopamine. We transduced the cells after 5 d of differentiation with 20  $\mu$ M retinoic acid and confirmed TH expression by western blot and immunocytochemistry compared with empty vector (CtrlVect)-transduced controls (Supplementary Fig. 1a–c). The TH-RREE transduced cells had measurable intracellular levels of L-DOPA, dopamine and DOPAC in the range of 25–200 fmol  $\mu$ g<sup>−1</sup>, whereas catecholamines were not detected in CtrlVect-transduced cells (Supplementary Fig. 1d), indicating that TH-RREE vector enhances catecholamine production.

We performed bilateral injections of TH-RREE vector into the SN of aged (10 month old) nontransgenic (NonTg) mice. This age was

selected because the mice expressing A53T mutant human  $\alpha$ -synuclein are asymptomatic and do not exhibit the characteristic motor phenotype derived from spinal cord degeneration<sup>32</sup>. The typical age of onset of this phenotype in our colony was approximately 18 months. At 5 months post-injection (mpi), TH expression was increased in both SN and striatum in NonTg TH-RREE mice compared with age-matched NonTg CtrlVect mice (Fig. 1a,b). TH-RREE significantly elevated striatal concentrations of L-DOPA and dopamine by 36% ( $P = 0.0235$ ) and 52% ( $P = 0.0137$ ), respectively, whereas DOPAC was not affected. Notably, 5-HT levels did not change, indicating that the effect was specific for the catecholamine neurotransmitter system (Fig. 1c). Consistent with elevated striatal dopamine, NonTg TH-RREE mice exhibited hyperactivity in open field-testing compared with NonTg CtrlVect mice (Fig. 1d). There was no difference in rotarod performance between the NonTg injection groups (Fig. 1e). These data indicate that the TH-RREE vector substantially enhanced dopamine levels fully 5 months following injection.

### Dopamine-induced neurodegeneration and motor deficit is dependent on $\alpha$ -synuclein expression

Bilateral injection of the TH-RREE vector into the SN of 10-month-old A53T mutant  $\alpha$ -synuclein mice also resulted in TH overexpression (Supplementary Fig. 2). However, in contrast with NonTg mice, A53T TH-RREE mice exhibited striatal degeneration and neuronal loss in the SN at 5 mpi. To circumvent detection of vector-encoded TH, we used another marker of dopaminergic neurons, VMAT2, to evaluate neuronal loss. A53T TH-RREE mice had fewer VMAT2-positive

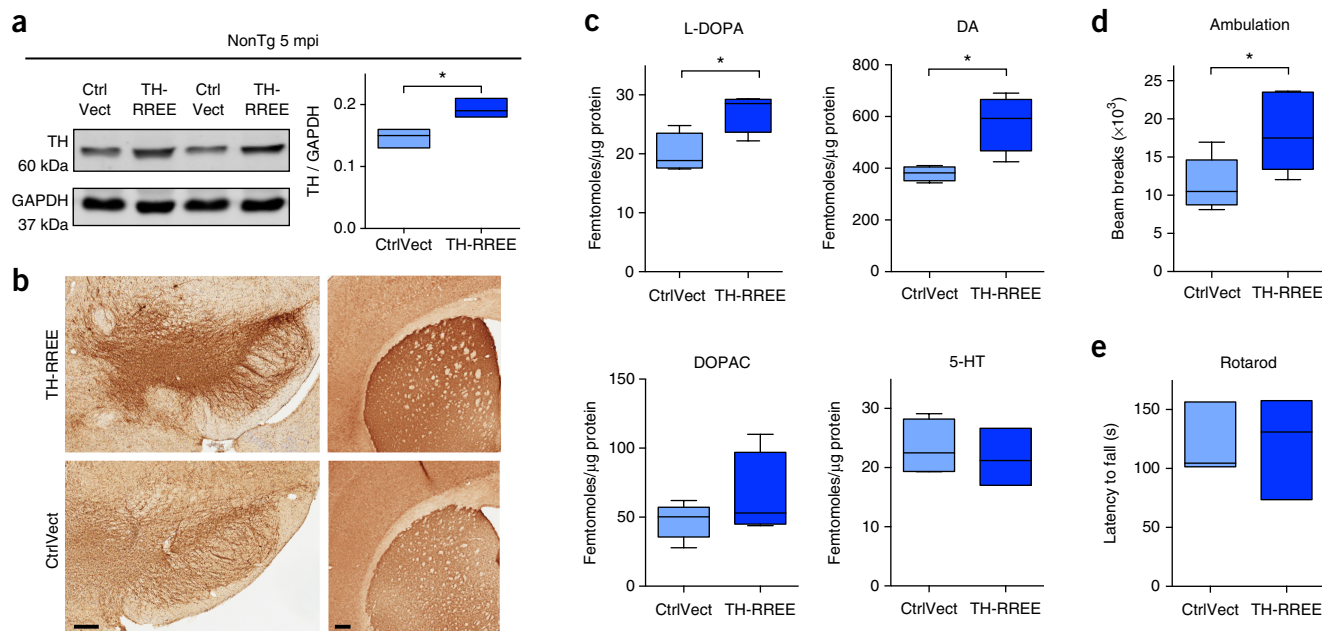


**Figure 1** TH-RREE lentiviral vector increases dopamine levels and causes hyperactivity in NonTg mice. (a) TH protein levels were increased in the striatum of TH-RREE-vector-injected mice relative to empty-vector-injected controls (CtrlVect) at 5 mpi. Densitometric analysis was conducted by normalizing TH to the GAPDH loading control. Blots are cropped; for full-length blots see Supplementary Figure 11 ( $n = 3$  mice per group,  $P = 0.0201$ ,  $t = 3.742$ , d.f. = 4; two-tailed unpaired Student's  $t$  test). (b) Increased TH expression was confirmed by immunohistochemistry in the SN (left) and striatum (right). Scale bars represent 200  $\mu$ m ( $n = 4$  mice per group). (c) TH overexpression significantly increased the steady state concentrations of striatal catecholamines L-DOPA and dopamine (DA), but did not alter DOPAC or 5-HT (L-DOPA,  $n = 4$  mice per group,  $P = 0.0235$ ,  $t = 3.017$ , d.f. = 6; DA,  $n = 4$  mice per group,  $P = 0.0137$ ,  $t = 3.445$ , d.f. = 6; DOPAC,  $n = 5$  mice for CtrlVect and  $n = 4$  mice for TH-RREE,  $P = 0.2713$ ,  $t = 1.194$ , d.f. = 7; 5-HT,  $n = 4$  mice for CtrlVect and  $n = 3$  mice for TH-RREE,  $P = 0.658$ ,  $t = 0.4703$ , d.f. = 5; two-tailed unpaired Student's  $t$  test). (d) TH-RREE injected NonTg mice exhibited greater locomotion as measured by open field activity ( $n = 5$  mice per group,  $P = 0.0399$ ,  $t = 2.451$ , d.f. = 8; two-tailed unpaired Student's  $t$  test). (e) There was no change in rotarod performance between the injection groups ( $n = 3$  mice per group,  $P = 0.9959$ ,  $t = 0.005455$ , d.f. = 4; two-tailed unpaired Student's  $t$  test). Box plots show median, 25th and 75th percentiles, and minimum and maximum values. \* $P < 0.05$ .

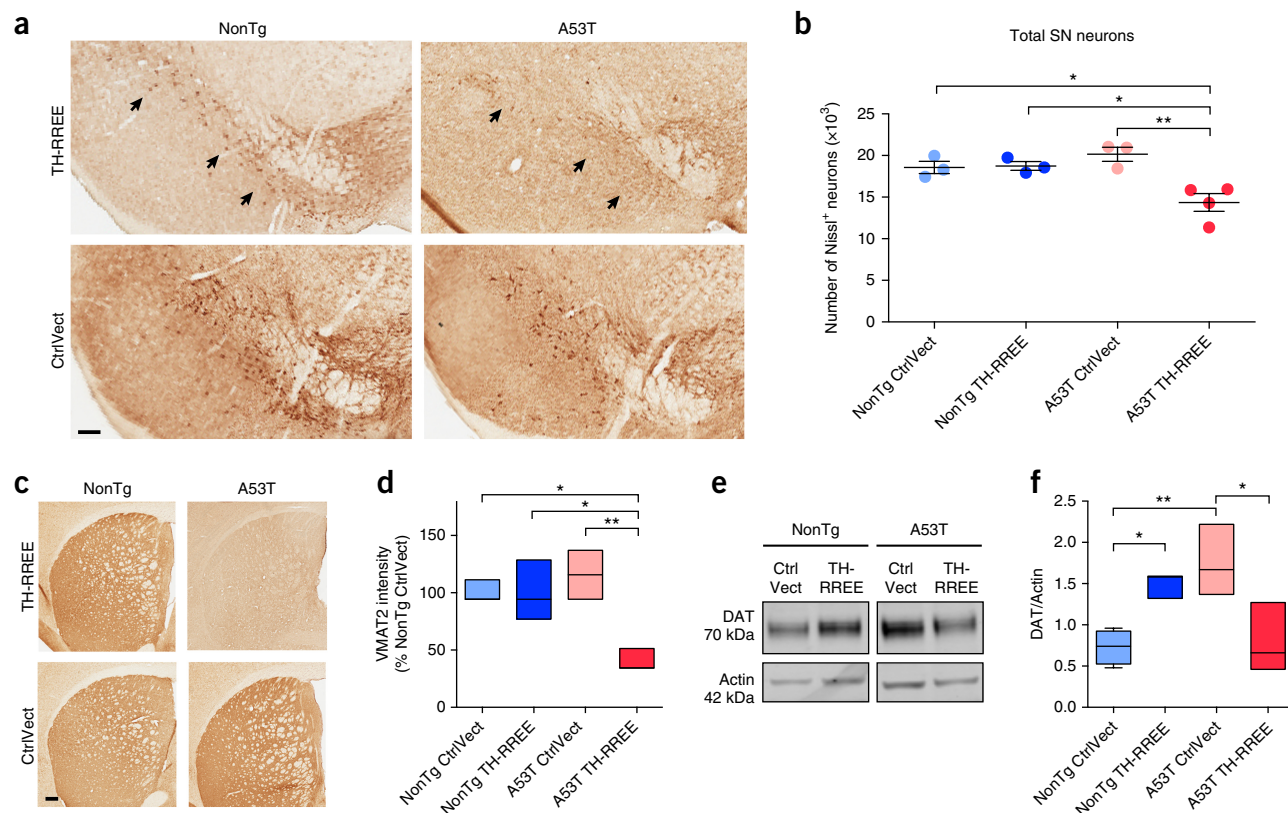


**Figure 2** Dopamine-induced neurodegeneration of the SN is dependent on  $\alpha$ -synuclein. **(a)** At 5 mpi, fewer VMAT2-positive cells (arrows) were present in the SN of A53T TH-RREE mice than in any other injection groups. Scale bar represents 100  $\mu$ m ( $n = 3$  mice per group). **(b)** Unbiased stereological counting of Nissl-positive neurons in the SN revealed a significant 25% loss of cells in A53T TH-RREE mice. The data are presented as mean  $\pm$  s.e.m. ( $n = 3$  mice per group except  $n = 4$  mice for A53T TH-RREE,  $P_{A53T \text{ TH-RREE versus A53T CtrlVect}} = 0.0049$ ,  $P_{A53T \text{ TH-RREE versus NonTg CtrlVect}} = 0.0316$ ,  $P_{A53T \text{ TH-RREE versus NonTg TH-RREE}} = 0.0253$ ,  $F_{(3,9)} = 8.810$ ; one-way ANOVA with Tukey's correction for multiple comparisons). **(c,d)** Histological analysis of VMAT2 staining in the striatum, with subtraction of background staining in the cortex, revealed severe dopaminergic denervation in A53T TH-RREE mice. Scale bar represents 200  $\mu$ m ( $n = 3$  mice per group,  $P_{A53T \text{ TH-RREE versus A53T CtrlVect}} = 0.0043$ ,  $P_{A53T \text{ TH-RREE versus NonTg CtrlVect}} = 0.0163$ ,  $P_{A53T \text{ TH-RREE versus NonTg TH-RREE}} = 0.0163$ ,  $F_{(3,8)} = 10.02$ ; one-way ANOVA with Tukey's correction for multiple comparisons). **(e,f)** Striatal DAT levels normalized to the actin loading control were increased in NonTg TH-RREE mice relative to NonTg CtrlVect, whereas DAT levels were decreased in A53T TH-RREE mice as compared to A53T CtrlVect. Blots are cropped; for full-length blots see **Supplementary Figure 11** ( $n = 3$  mice per group except  $n = 4$  mice for NonTg CtrlVect,  $P_{A53T \text{ TH-RREE versus A53T CtrlVect}} = 0.0211$ ,  $P_{A53T \text{ CtrlVect versus NonTg CtrlVect}} = 0.0097$ ,  $P_{\text{NonTg TH-RREE versus NonTg CtrlVect}} = 0.0466$ ,  $F_{(3,9)} = 8.411$ ; one-way ANOVA with Tukey's correction for multiple comparisons). Box plots show median, 25th and 75th percentiles, and minimum and maximum values. \* $P < 0.05$ , \*\* $P < 0.01$ .

cells in the SN than any of the other injection groups (**Fig. 2a**). We quantified the loss of neurons using unbiased stereological counting of Nissl cells, which revealed a significant 25% reduction in A53T TH-RREE mice compared with controls (**Fig. 2b**). The number of neurons quantified in age-matched A53T CtrlVect, as well as NonTg CtrlVect and NonTg TH-RREE mice, was typical for the mouse SN<sup>33</sup>, indicating that neurodegeneration had not occurred in these mice (**Fig. 2b**).

The degeneration of cell bodies was accompanied by a significant 62% decrease in VMAT2 staining in the striatum of A53T TH-RREE mice, indicating that there was a severe loss of dopaminergic nerve terminals (**Fig. 2c,d**). Denervation of the striatum was further corroborated by quantification of dopamine transporter (DAT) levels, which revealed a significant 55% decline ( $P = 0.0211$ ) in A53T TH-RREE mice compared with A53T CtrlVect. In contrast, the levels of DAT were twofold higher in NonTg TH-RREE than in NonTg CtrlVect mice (**Fig. 2e,f**). DAT upregulation may serve to compensate for increased dopamine levels, and may not be apparent in A53T TH-RREE mice as a result of the substantial loss of dopaminergic terminals. The injury in A53T mice appears to be primarily presynaptic in that levels of D1

receptors remained unchanged (**Supplementary Fig. 3a,b**). Levels of dopamine- and cAMP-regulated phosphoprotein-32 (DARPP-32), which serves as an important signaling molecule in spiny projection neurons, were also unaffected (**Supplementary Fig. 3a,c**).

To further investigate the progressive degenerative phenotype in A53T TH-RREE mice, we quantified the total number of SN neurons at the earlier time point of 2.5 mpi. No difference was observed between A53T CtrlVect and TH-RREE mice, indicating that cell loss had not yet occurred (**Fig. 3a**). Despite the maintenance of neuronal cell bodies, striatal VMAT2 levels were decreased by 25% (**Fig. 3b**), revealing a milder loss of nerve terminals than at the later time point of 5 mpi (**Fig. 2c–d**). Consistent with progressive degeneration of synapses, we noted a time-dependent decline of striatal dopamine content in A53T TH-RREE mice. At 2.5 mpi, dopamine was increased significantly by 71% compared with age-matched A53T CtrlVect mice as a result of mutant TH expression (**Fig. 3c**). However, A53T TH-RREE mice subsequently exhibited a 37% drop in dopamine concentration between 2.5 and 5 mpi, whereas A53T CtrlVect mice showed no change during the same period (**Fig. 3c**).



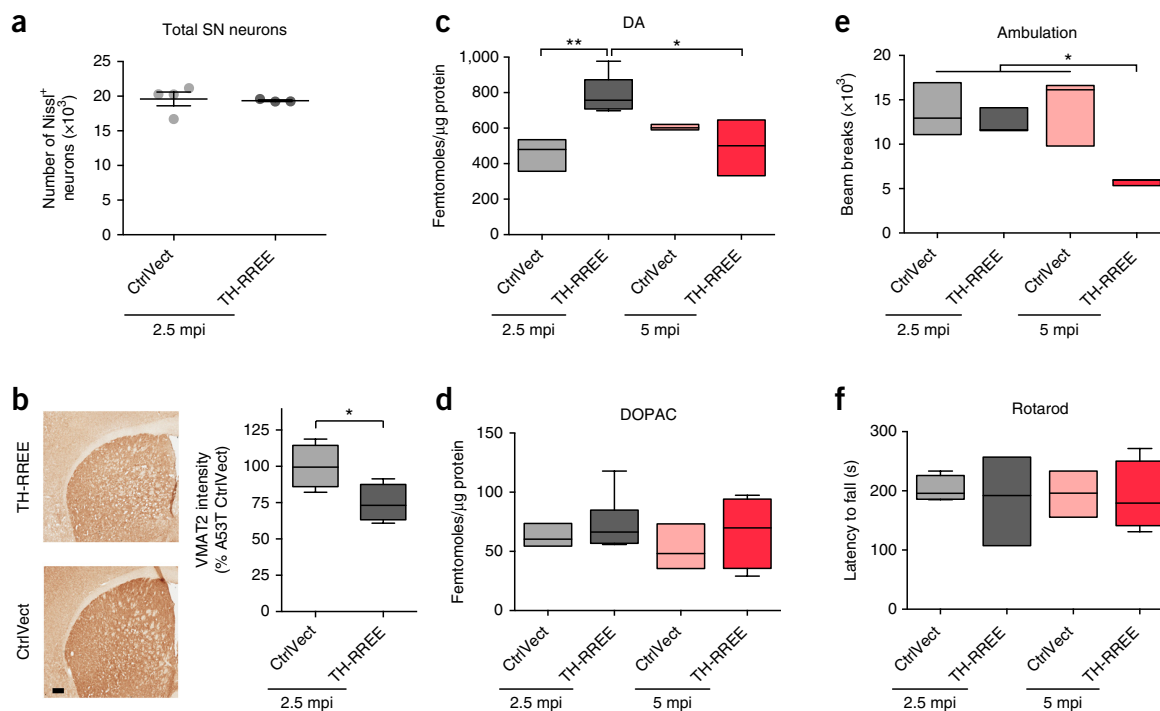


**Figure 3** Dopaminergic neurodegeneration in A53T TH-RREE mice is progressive and ultimately leads to locomotor deficit. **(a)** At the early time point of 2.5 mpi, A53T TH-RREE mice did not yet exhibit loss of neuronal cell bodies in the SN. The data are presented as mean  $\pm$  s.e.m. ( $n = 4$  mice for CtrlVect and  $n = 3$  mice for TH-RREE,  $P = 0.8453$ ,  $t = 0.2055$ , d.f. = 5; two-tailed unpaired Student's  $t$  test). **(b)** VMAT2 staining in the striatum revealed a modest loss of terminals, suggesting that dopaminergic synapses had degenerated before overt cell death. Scale bar represents 200  $\mu$ m ( $n = 4$  mice per group,  $P = 0.0424$ ,  $t = 2.569$ , d.f. = 6; two-tailed unpaired Student's  $t$  test). **(c)** A53T TH-RREE mice exhibited an elevation of dopamine (DA) levels only transiently, with an initial increase of 71% at 2.5 mpi compared with age-matched A53T CtrlVect mice. Subsequently, however, A53T TH-RREE mice underwent a significant 37% drop in striatal dopamine between 2.5 and 5 mpi, which was not observed in A53T CtrlVect mice ( $n = 3$  mice per group except  $n = 5$  mice for TH-RREE 2.5 mpi,  $P_{\text{TH-RREE 2.5 mpi versus CtrlVect 2.5 mpi}} = 0.0092$ ,  $P_{\text{TH-RREE 2.5 mpi versus TH-RREE 5 mpi}} = 0.0187$ ,  $F_{(3,10)} = 7.460$ ; one-way ANOVA with Tukey's correction for multiple comparisons). **(d)** Levels of DOPAC in the striatum remained unchanged over time regardless of lentiviral treatment. (CtrlVect,  $n = 3$  mice per group; TH-RREE,  $n = 6$  mice for 2.5 mpi and  $n = 4$  mice for 5 mpi,  $F_{(3,12)} = 0.5481$ ; one-way ANOVA with Tukey's correction for multiple comparisons). **(e)** Consistent with a late-onset depletion of dopamine in the striatum, from 2.5 to 5 mpi, A53T TH-RREE mice developed a reduction in locomotor activity that was not observed in CtrlVect mice ( $n = 3$  mice per group,  $P_{\text{TH-RREE 5 mpi versus CtrlVect 5 mpi}} = 0.0152$ ,  $P_{\text{TH-RREE 5 mpi versus TH-RREE 2.5 mpi}} = 0.0488$ ,  $P_{\text{TH-RREE 5 mpi versus CtrlVect 2.5 mpi}} = 0.0213$ ,  $F_{(3,8)} = 7.107$ ; one-way ANOVA with Tukey's correction for multiple comparisons). **(f)** The motor deficit in A53T TH-RREE mice was not severe enough to affect coordination or balance, as rotarod performance remained intact ( $n = 4$  mice per group except  $n = 3$  mice for TH-RREE 2.5 mpi and  $n = 3$  mice for CtrlVect 5 mpi,  $F_{(3,10)} = 0.07172$ ; one-way ANOVA with Tukey's correction for multiple comparisons). Box plots show median, 25th and 75th percentiles, and minimum and maximum values. \* $P < 0.05$ , \*\* $P < 0.01$ .

The reduction in dopamine levels cannot be explained by increased conversion to DOPAC, as levels of this metabolite remained unchanged from 2.5 to 5 mpi (Fig. 3d). We also did not detect an increase in dopamine-protein adducts by near infrared fluorescence (Supplementary Fig. 4). Rather, the loss of dopamine is likely a result of the ongoing nigrostriatal degeneration documented in these mice. Concomitant with the decrease in dopamine levels, A53T TH-RREE mice exhibited a significant impairment in ambulatory activity that was not apparent at 2.5 mpi, but emerged by 5 mpi (Fig. 3e). Performance on the rotarod remained intact, suggesting that balance and coordination were not disrupted (Fig. 3f). Collectively, the results indicate that enhanced production of dopamine promotes the progressive degeneration of dopaminergic neurons and a specific motor deficit in mice that express A53T  $\alpha$ -synuclein, but not in NonTg mice.

#### Dopamine modifies $\alpha$ -synuclein oligomer conformations in A53T mice

These data indicate that increased steady state levels of dopamine result in neurotoxicity in an  $\alpha$ -synuclein-dependent manner. To investigate

possible mechanisms, we examined the influence of dopamine on  $\alpha$ -synuclein aggregation and, in particular, the kinetic stabilization of potentially toxic  $\alpha$ -synuclein oligomers. The presence of Lewy-body-like inclusions in circumscribed regions, including the brainstem of aged A53T mice, has been well-documented<sup>32</sup>.  $\alpha$ -Synuclein-positive inclusions were indeed detected in the brainstem of A53T TH-RREE mice at 5 mpi (age 15 months), similar to age-matched A53T CtrlVect mice (Supplementary Fig. 5a). In contrast, the SN is known to remain devoid of inclusions during the lifespan of A53T mice<sup>32</sup>. Expression of TH-RREE vector did not induce  $\alpha$ -synuclein inclusion formation or alter levels or conformations of detergent-insoluble  $\alpha$ -synuclein in the SN at 5 mpi (Supplementary Fig. 5).

Examination of detergent-soluble  $\alpha$ -synuclein extracted from SN of A53T mice at 5 mpi revealed substantial alterations in the quantities and conformations of  $\alpha$ -synuclein species as a result of dopamine elevation. A53T TH-RREE mice had a significant 22% reduction in monomeric human  $\alpha$ -synuclein compared with A53T CtrlVect mice (Fig. 4a,b). Following fractionation of the soluble SN extract by native size exclusion chromatography (SEC), we detected the presence of

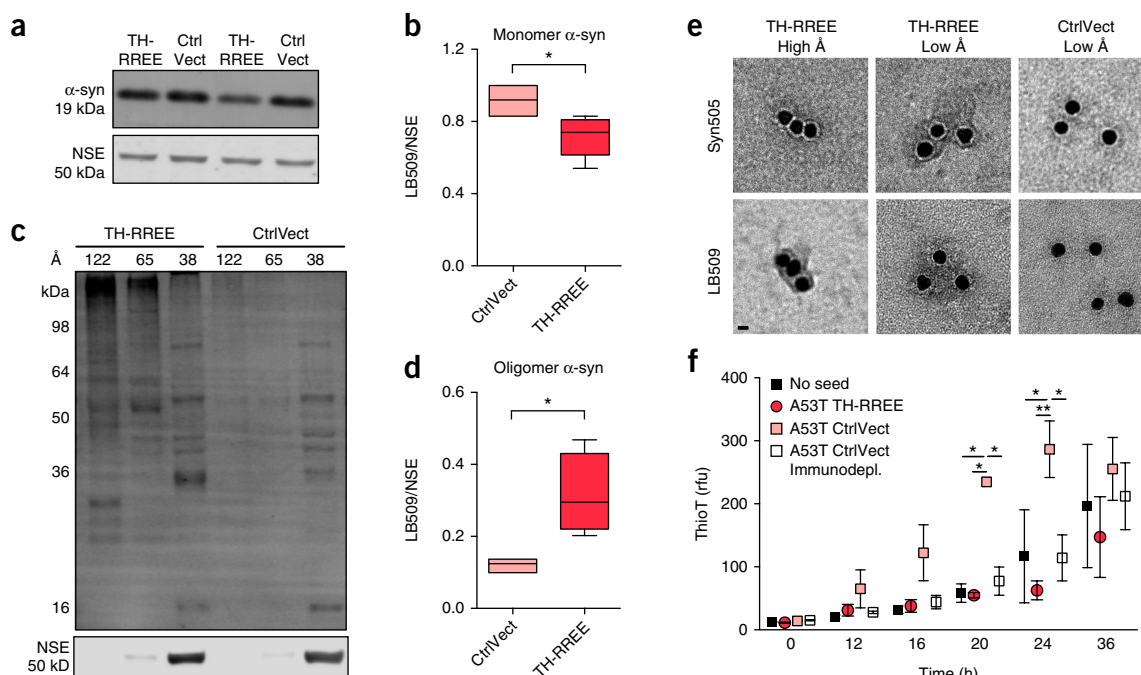


**Figure 4** Dopamine induces conformationally distinct  $\alpha$ -synuclein oligomers in the mouse brain. (a–d) The SN of A53T TH-RREE and A53T CtrlVect mice at 5 mpi was extracted with 1% Triton and the soluble fraction was analyzed by SDS-PAGE (a,b). The soluble extract was further subjected to native SEC and fractions corresponding to 31–38 Å, 41–65 Å and 72–122 Å were pooled and analyzed by SDS-PAGE (c,d). Neural specific enolase (NSE) was used as a loading control. The quantification revealed a decrease in soluble  $\alpha$ -synuclein monomer and a corresponding increase in  $\alpha$ -synuclein oligomers in A53T TH-RREE compared with A53T CtrlVect. The oligomer species in A53T TH-RREE mice were present in higher angstrom fractions than in controls and had a range of molecular weights. Monomer  $\alpha$ -synuclein and NSE blots are cropped; for full-length blots, see **Supplementary Figure 11** (monomer,  $n = 3$  mice for CtrlVect and  $n = 5$  mice for TH-RREE,  $P = 0.0401$ ,  $t = 2.611$ , d.f. = 6; Oligomer,  $n = 3$  mice for CtrlVect and  $n = 4$  mice for TH-RREE,  $P = 0.0338$ ,  $t = 2.900$ , d.f. = 5; two-tailed unpaired Student's  $t$  test). (e) Immunoelectron microscopy on low-(41–65) and high-angstrom (72–122) fractions from A53T mice using Syn505 (N-terminal) and LB509 (C-terminal)  $\alpha$ -synuclein antibodies, with 10-nm gold-conjugated secondary. Scale bar represents 10 nm ( $n = 3$  mice per group). (f) Pooled oligomeric fractions (41–122 Å) from indicated mice were added to aggregation reactions with fresh recombinant  $\alpha$ -synuclein, and fibril formation was monitored by Thioflavin T (ThioT). Prior immunodepletion of  $\alpha$ -synuclein from A53T CtrlVect fractions was performed as a control. rfu, relative fluorescence units. The data are presented as mean  $\pm$  s.e.m. ( $n = 3$  mice per group except  $n = 4$  mice for no seed and  $n = 4$  mice for immunodepletion;  $P_{\text{A53T CtrlVect 20 h versus no seed 20 h}} = 0.0114$ ,  $P_{\text{A53T CtrlVect 20 h versus A53T TH-RREE 20 h}} = 0.0172$ ,  $P_{\text{A53T CtrlVect 20 h versus A53T CtrlVect Immunodepl. 20 h}} = 0.0292$ ,  $P_{\text{A53T CtrlVect 24 h versus no seed 24 h}} = 0.0158$ ,  $P_{\text{A53T CtrlVect 24 h versus A53T TH-RREE 24 h}} = 0.0019$ ,  $P_{\text{A53T CtrlVect 24 h versus A53T CtrlVect Immunodepl. 24 h}} = 0.0139$ ,  $F_{(3,10)} = 4.563$ ; repeated measures two-way ANOVA with Tukey's correction for multiple comparisons). Box plots show median, 25th and 75th percentiles, and minimum and maximum values. \* $P < 0.05$ , \*\* $P < 0.01$ .

various oligomeric  $\alpha$ -synuclein species of different molecular weights (Fig. 4c). Quantification of total oligomeric species revealed a significant increase in A53T TH-RREE mice, greater than twofold above that in A53T CtrlVect mice (Fig. 4d). To characterize the oligomers, we used multiple  $\alpha$ -synuclein antibodies and a combination of SDS-PAGE, immunoelectron microscopy and biochemical assays. In A53T CtrlVect mice, oligomers had Stokes radii of up to 65 Å and ranged in molecular weight from 36 to 80 kDa (Fig. 4c and **Supplementary Fig. 6a,b**), consistent with previous observations<sup>34</sup>. However, in addition to these low-angstrom species, larger species of up to 122 Å were detected in A53T TH-RREE mice. On 12% SDS-PAGE, these species migrated as dimers, trimers and high-molecular-weight polymers stable to SDS and heat, consistent with the presence of oxidized and crosslinked species<sup>35</sup>. The appearance of unique, high-angstrom species in A53T TH-RREE mice was observed with multiple  $\alpha$ -synuclein antibodies that recognize N- or C-terminal epitopes (Fig. 4c and **Supplementary Fig. 6a,b**). Moreover, analysis of quinone-associated protein by near-infrared fluorescence revealed that only the high-angstrom oligomeric fractions from A53T TH-RREE mice were positive, supporting a direct interaction of dopamine and  $\alpha$ -synuclein oligomers in these mice (**Supplementary Fig. 6c**).

Further structural analysis of oligomers isolated from high-(72–122) or low-angstrom (41–65) SEC fractions was undertaken by immunoelectron microscopy. Oligomers typically appeared as clusters with >2 gold particles in both high- and low-angstrom fractions from A53T TH-RREE mice, as well as low-angstrom fractions from A53T CtrlVect mice. The species were labeled with  $\alpha$ -synuclein antibodies directed at either the N- or C terminus, indicating that both ends were exposed (Fig. 4e). Clusters of >2 gold particles were not observed in high-angstrom fractions from A53T CtrlVect mice or fractions from A53T TH-RREE mice that were immunodepleted of  $\alpha$ -synuclein before imaging. Similar to mouse-derived oligomers, oligomers generated from incubating purified recombinant human wild-type  $\alpha$ -synuclein with dopamine *in vitro* migrated as 36- to >98-kDa bands on SDS-PAGE and were recognized by both N- and C-terminally directed  $\alpha$ -synuclein antibodies in western blots and by immunoelectron microscopy (**Supplementary Fig. 7c,d**). Electron microscopy imaging of the recombinant oligomers revealed clusters of >2 gold particles as observed in oligomer fractions from mouse SN (**Supplementary Fig. 7d**).

Given that there is growing evidence for prion-like spreading of  $\alpha$ -synuclein pathology in disease<sup>36</sup>, we investigated whether dopamine

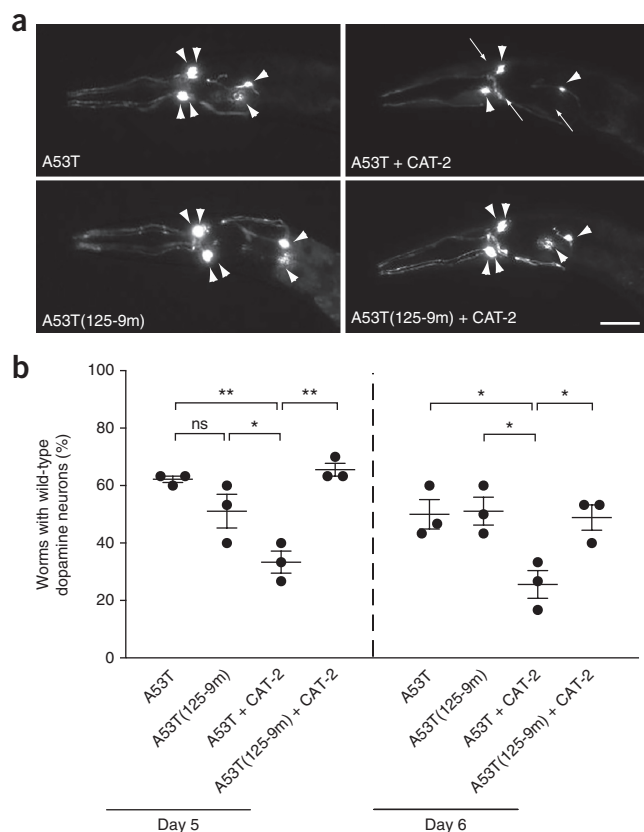


**Figure 5** *C. elegans* expressing A53T  $\alpha$ -synuclein lacking the site of interaction with dopamine are resistant to dopamine neurotoxicity. **(a,b)** Expression of A53T human  $\alpha$ -synuclein in dopaminergic neurons of *C. elegans* resulted in 62% of worms with wild-type dopamine neurons at day 5 post-hatching, and 50% at day 6 post-hatching. Overexpression of CAT-2 in A53T worms significantly exacerbated toxicity at both time points, whereas coexpression of CAT-2 with A53T  $\alpha$ -synuclein mutated at the site of interaction with dopamine (A53T(125-9m)) showed significant resistance to CAT-2 induced toxicity. Representative images from day 5 post-hatching are shown in **a**, with intact neurons marked by arrowheads and degenerating or missing neurons by arrows. Scale bar represents 10  $\mu$ m. ns, not significant. The data are presented as mean  $\pm$  s.e.m. ( $n$  = 30 worms per genotype per replicate, 3 independent replicates,  $P_{A53T + CAT-2 \text{ Day 5 versus A53T Day 5}} = 0.0026$ ,  $P_{A53T + CAT-2 \text{ Day 5 versus A53T(125-9m) Day 5}} = 0.0393$ ,  $P_{A53T + CAT-2 \text{ Day 5 versus A53T(125-9m) + CAT-2 Day 5}} = 0.0013$ ,  $F_{(3,8)} = 15.19$ ;  $P_{A53T + CAT-2 \text{ Day 6 versus A53T Day 6}} = 0.029$ ,  $P_{A53T + CAT-2 \text{ Day 6 versus A53T(125-9m) Day 6}} = 0.0232$ ,  $P_{A53T + CAT-2 \text{ Day 6 versus A53T(125-9m) + CAT-2 Day 6}} = 0.0365$ ,  $F_{(3,8)} = 6.488$ ; one-way ANOVA on each time point with Tukey's correction for multiple comparisons). \* $P < 0.05$ , \*\* $P < 0.01$ .

promotes *in vivo* formation of oligomeric species with the capacity for templated propagation.  $\alpha$ -synuclein oligomers extracted from A53T TH-RREE or A53T CtrlVect mice (pooled 41–122-Å SEC fractions) were monitored in a seeding assay with fresh recombinant  $\alpha$ -synuclein *in vitro*. In the case of A53T CtrlVect mice, oligomers efficiently seeded aggregation relative to the no-seed condition, as measured by Thioflavin T (Fig. 4f). Notably, this effect was abolished by prior immunodepletion of  $\alpha$ -synuclein from the SEC fractions. In contrast, the same fractions from TH-RREE mice were unable to act as seeds (Fig. 4f), suggesting that seeding-competent species were not retained following the interaction of  $\alpha$ -synuclein with dopamine *in vivo*. We also did not detect dopamine-modified oligomers in the motor cortex of A53T TH-RREE mice (Supplementary Fig. 8), suggesting that these species do not spread trans-synaptically. Collectively,

these data indicate that dopamine promotes the generation of conformationally and functionally modified  $\alpha$ -synuclein oligomeric species in the mouse brain.

To further establish the link between dopamine-induced oligomers and toxicity, we exposed primary neuronal cultures to recombinant  $\alpha$ -synuclein oligomers generated in the presence of dopamine *in vitro*. Exogenous  $\alpha$ -synuclein from oligomer preparations had become internalized in neurons and localized to neurites by 2 weeks post-treatment (Supplementary Fig. 9a). At this time point, we evaluated cells for viability using Calcein AM and propidium iodide (PI) dyes. Exposure of neurons to 1  $\mu$ M dopamine-incubated  $\alpha$ -synuclein induced a significant 44% reduction in Calcein-positive, PI-negative cells relative to phosphate-buffered saline (PBS)-treated controls (Supplementary Fig. 9b,c). Treatment with equivalent doses of monomeric  $\alpha$ -synuclein, or dopamine that had been incubated under aggregation conditions without  $\alpha$ -synuclein, did not reduce cell viability (Supplementary Fig. 9b,c). The observed neurotoxicity can therefore be attributed specifically to  $\alpha$ -synuclein oligomers, consistent with our findings *in vivo* linking dopamine-modified species with severe nigrostriatal degeneration.

### Disrupting the interaction of dopamine and $\alpha$ -synuclein mitigates neurotoxicity in *C. elegans*

To gain further mechanistic insight into the synergistic toxicity of dopamine and  $\alpha$ -synuclein, we took advantage of the genetic tractability of the nematode model system *Caenorhabditis elegans*. Previous studies have shown that expressing human wild-type or PD-linked mutants of  $\alpha$ -synuclein in dopaminergic neurons of *C. elegans* causes progressive age-dependent neurodegeneration<sup>37–40</sup>. Overexpression of the TH homolog CAT-2 also induces dopamine neuron loss in worms<sup>38</sup>. To test the combined effect of these factors on neuronal health, we first generated transgenic worms expressing human A53T  $\alpha$ -synuclein under the control of the worm dopamine transporter (*dat-1*) promoter. *C. elegans* hermaphrodites have precisely eight dopamine neurons, which we visualized by coexpressing *P<sub>dat-1</sub>::GFP*. Consistent with previous *C. elegans* models of A53T  $\alpha$ -synuclein toxicity, we documented that 62% and 50% of A53T worms maintained normal dopamine neurons on days 5 and 6 post-hatching, respectively (Fig. 5). Notably, CAT-2 overexpression in A53T worms significantly exacerbated the degeneration of dopamine neurons, with only 33% and 26% of worms exhibiting normal neurons at days 5 and 6, respectively (Fig. 5). These data are consistent with our observations in the A53T TH-RREE mouse model and suggest that neuronal susceptibility to dopamine/ $\alpha$ -synuclein toxicity is conserved.

We next investigated whether mutating  $\alpha$ -synuclein at the site of interaction with dopamine would rescue neurons from degeneration. Mutation of the Y<sub>125</sub>EMPS<sub>129</sub> motif in the C terminus of  $\alpha$ -synuclein to F<sub>125</sub>AAFA<sub>129</sub> abolishes the interaction with dopamine and inhibits dopamine-mediated stabilization of oligomers<sup>25,27</sup>. Transgenic worms expressing A53T  $\alpha$ -synuclein with the F<sub>125</sub>AAFA<sub>129</sub> mutation [A53T(125-9m)] at similar levels as A53T  $\alpha$ -synuclein showed no difference in dopamine neuron degeneration compared with A53T worms (Fig. 5 and Supplementary Fig. 10). However, A53T(125-9m) worms displayed complete resistance to CAT-2-induced neurodegeneration, with the percentage of worms exhibiting normal dopamine neurons restored to 66% and 49% on days 5 and 6, respectively (Fig. 5). These findings suggest that the specific interaction of dopamine with the C terminus of  $\alpha$ -synuclein is a critical contributor to the degeneration of dopamine neurons *in vivo*. The demonstration of this phenomenon in two *in vivo* platforms (worms and mice) strongly supports a role for dopamine-induced oligomers in the mechanism of neurotoxicity.



## DISCUSSION

We used a new approach to enhance nigrostriatal dopamine levels in A53T mutant human  $\alpha$ -synuclein transgenic mice. In this well-characterized mouse model, the SN does not develop  $\alpha$ -synuclein inclusions and does not undergo neuronal cell loss<sup>32</sup>. However, elevation of dopamine levels in the A53T mice induced substantial nigrostriatal degeneration and a previously undescribed locomotor impairment. Neurodegeneration was not observed in NonTg mice receiving the same treatment, indicating that dopamine-induced toxicity is dependent on  $\alpha$ -synuclein. To the best of our knowledge, this is also the first demonstration that dopamine promotes  $\alpha$ -synuclein oligomerization *in vivo* and that disrupting the ability of dopamine to stabilize/modify oligomers rescues neurons from dopamine toxicity. Taken together, these findings suggest that dopamine-induced  $\alpha$ -synuclein oligomers may be a promising new target for PD treatment.

Dopamine has long been considered a contributor to the death of dopaminergic neurons in disease<sup>3</sup>. At cytosolic pH, dopamine auto-oxidizes to form reactive quinone species, hydrogen peroxide and other electrophiles<sup>2</sup>. The notion that dopamine may be neurotoxic has resulted in the widespread practice of 'DOPA sparing', which delays administration of the highly effective symptomatic therapy L-DOPA until more advanced stages of the disease. Although there is presently no conclusive evidence indicating that L-DOPA accelerates PD progression, clinical trials have provided mixed results and the issue of L-DOPA toxicity remains, unfortunately, unresolved<sup>41,42</sup>. Despite the importance of investigating catecholamine toxicity, there are few studies in animal models. Single high-dose injections of dopamine into the striatum of rats have been shown to be acutely toxic in the short timeframe of 1 week<sup>7</sup>. Other reports have shown that redistribution of endogenous dopamine to the cytosol is associated with toxicity in VMAT2 mutant mice<sup>8,9</sup>. However, the long-term effects of increasing nigrostriatal dopamine levels remain unknown.

Our experiments represent the first investigation of dopamine toxicity by chronic enhancement of dopamine synthesis in mice. By expressing mutant TH that is insensitive to feedback inhibition by dopamine<sup>26,27,31</sup>, we found that striatal dopamine in NonTg mice was increased by over 50%. To our surprise, this substantial perturbation of dopamine homeostasis was insufficient to induce degeneration. NonTg TH-RREE mice maintained a normal number of SN neurons, intact synaptic contacts with the striatum and robust motor coordination/balance. The excess dopamine was likely released into the synapse, leading to the observed hyperactivity, which is consistent with other studies<sup>43</sup>. It is possible the excess dopamine was well tolerated as a result of compensatory upregulation of metabolic enzymes and transporters; indeed, there was a substantial increase in DAT levels in these mice.

$\alpha$ -synuclein has been independently linked to PD through dominantly inherited mutations and multiplications of the SNCA gene<sup>10–17</sup>, and by the presence of aggregated  $\alpha$ -synuclein in Lewy bodies and Lewy neurite inclusions<sup>18,19</sup>. However, efforts to model PD by  $\alpha$ -synuclein overexpression in transgenic mice have often resulted in a lack of inclusion pathology and neurodegenerative changes in the SN. Dopaminergic neurons are entirely spared in the A53T transgenic mouse model that we used<sup>32</sup>, and we documented a normal complement of neuronal cell bodies and terminals and a lack of intraneuronal  $\alpha$ -synuclein inclusions in the SN in A53T CtrlVect mice. This may be related to several factors, including the fact that mouse  $\alpha$ -synuclein naturally has a threonine at position 53. *In vitro*, mouse  $\alpha$ -synuclein fibrillizes more rapidly than human wild-type or A53T  $\alpha$ -synuclein, and yet aged mice do not spontaneously develop  $\alpha$ -synuclein inclusions or a PD-like disorder<sup>44</sup>. It is likely that mice have evolved

protective mechanisms against  $\alpha$ -synuclein aggregation, such as an enhanced ability to maintain  $\alpha$ -synuclein in a physiological lipid- or protein-bound state, and that these mechanisms may counteract efforts to initiate disease by transgenic  $\alpha$ -synuclein expression.

Our study offers another possible explanation for the challenges of producing SN neurodegeneration in  $\alpha$ -synuclein transgenic mice: lack of dopamine dysregulation. In stark contrast with NonTg mice, elevation of dopamine levels in A53T mice resulted in progressive nigrostriatal degeneration with locomotor impairment, markedly improving this mouse as a model of PD. Similarly, coexpression of CAT-2 and A53T  $\alpha$ -synuclein in *C. elegans* induced more severe dopamine neuron degeneration than A53T  $\alpha$ -synuclein expression alone. These findings are consistent with a limited number of studies reporting toxicity associated with the convergence of dopamine and  $\alpha$ -synuclein. In the case of VMAT2-deficient mice, loss of SN neurons was only observed in animals on a normal  $\alpha$ -synuclein background, whereas identical reduction of VMAT2 in animals with *Snc*a gene locus deletion did not result in cell loss<sup>8,9,45</sup>. In *C. elegans* expressing wild-type human  $\alpha$ -synuclein, increasing cytosolic dopamine by mutation of the worm homolog of VMAT2 accelerated neurodegeneration. Conversely, protection from neuronal loss has been reported for worms expressing wild-type human  $\alpha$ -synuclein and a nonfunctional mutant of CAT-2 that prevents dopamine synthesis<sup>40</sup>. In addition, in rodent midbrain cultures, elevating cytosolic dopamine concentration reduces dopaminergic cell survival, and this effect is dependent on  $\alpha$ -synuclein<sup>46</sup>.

The synergistic toxicity of dopamine and  $\alpha$ -synuclein may be mediated by  $\alpha$ -synuclein oligomers, which are thought to be neurotoxic species. Lentiviral vector delivery of artificial  $\alpha$ -synuclein variants with enhanced oligomerization into the rat SN resulted in the selective loss of dopaminergic cells<sup>47</sup>. Similarly, artificial mutants with impaired  $\beta$ -sheet structure and increased propensity to form oligomers induced degeneration of dopaminergic nerve terminals in worms and overt dopaminergic cell loss in flies<sup>39</sup>. In addition, oligomer-containing extracts from A53T transgenic mice were toxic when applied to primary mouse cortical cultures<sup>34</sup>. Although it is known that oxidized dopamine kinetically stabilizes soluble  $\alpha$ -synuclein oligomers in cell-free systems<sup>24,25</sup> and in SH-SY5Y cultures<sup>26,27</sup>, the toxicity of these species is largely unexplored. Evidence from studies conducted *in vitro* suggests that dopamine-induced oligomers can block their own degradation and that of other substrates by chaperone-mediated autophagy<sup>29</sup>, and can reduce neurotransmitter release by inhibition of SNARE complex formation<sup>30</sup>. In human fetal dopaminergic cultures, reduced viability was linked to endogenous dopamine and the accumulation of soluble  $\alpha$ -synuclein protein complexes<sup>48</sup>.

Notably, the effects of dopamine on  $\alpha$ -synuclein oligomerization *in vivo* have not been investigated. Thus, we sought to determine whether A53T TH-RREE mice had alterations in oligomer biochemical and/or functional properties. Soluble  $\alpha$ -synuclein oligomers were extracted from the SN and enriched by SEC under non-denaturing conditions to preserve native conformations. Increasing dopamine resulted in greater total levels of  $\alpha$ -synuclein oligomers detected by western blot. The oligomers included species with Stokes radii of up to 65 Å that were also detected in A53T CtrlVect mice, consistent with previous characterization of oligomers in aged A53T mice<sup>34</sup>. Larger oligomers of up to 122 Å were uniquely observed in A53T TH-RREE mice, suggesting that dopamine is capable of modifying oligomer conformations. These species may reflect dopamine-induced remodeling of existing oligomers and/or formation of oligomers from  $\alpha$ -synuclein monomers *de novo*. In addition, oligomers with larger Stokes radii may contain a greater number of monomer units than lower angstrom species, and/or occupy less compacted arrangements.

Multiple biochemical and imaging approaches were employed to characterize the oligomers extracted from the SN. In addition to well-established methods such as western blotting and SEC, immunoelectron microscopy was performed on SEC fractions to visualize mouse-derived  $\alpha$ -synuclein oligomers. Currently, there is no accepted method of specifically imaging  $\alpha$ -synuclein oligomers in brain tissue *in situ*. However, with our approach, we were able to identify and image oligomers of known Stokes radii. Oligomer species from both A53T TH-RREE and A53T CtrlVect mice were labeled with antibodies directed at the N- or C terminus of  $\alpha$ -synuclein, suggesting that epitopes at both ends of the protein were exposed. These epitopes were also exposed in soluble  $\alpha$ -synuclein oligomers generated with dopamine *in vitro*, consistent with previous imaging by immunoelectron microscopy<sup>25</sup>. Furthermore, LB509 and Syn505 antibodies are known to react robustly with  $\alpha$ -synuclein in pathological inclusions in human disease brain<sup>19,32</sup>. The reactivity of both mouse-derived and recombinant oligomers with these antibodies suggests that they may share disease-associated conformations.

Unlike the  $\alpha$ -synuclein species extracted from A53T CtrlVect mice, oligomers from A53T TH-RREE mice were unable to act as seeds for  $\alpha$ -synuclein fibrillization *in vitro*. In addition, we did not detect dopamine-modified oligomers in cortical tissue from A53T TH-RREE mice. These data argue against both intracellular and intercellular prion-like propagation of these species. Although  $\alpha$ -synuclein aggregates that exhibit prion-like behavior have been shown in many contexts to be cytotoxic<sup>34,36</sup>, seeding ability is neither necessary nor sufficient for toxicity. In a comparison of different oligomer species generated *in vitro*,  $\alpha$ -synuclein oligomers that were toxic to SH-SY5Y cultures were also incapable of seeding intracellular aggregation of  $\alpha$ -synuclein. Conversely, seeding-competent oligomers were found to be non-toxic when applied to SH-SY5Y cells<sup>49</sup>. Although the spread of  $\alpha$ -synuclein pathology in PD may primarily be driven by self-replicating seeding and cell-to-cell transmission, toxicity may depend on the interaction of aggregates with cell-type-specific factors. In this regard, dopamine may act as an enhancer of oligomer toxicity. Moreover, dopamine-modified species may resist sequestration into non-toxic fibrils or inclusions, and may therefore be available to participate in pathological interactions that ultimately lead to neuron death.

Although the mouse data clearly demonstrate an association between the neurodegenerative/locomotor disease phenotype and the presence of modified and more abundant  $\alpha$ -synuclein oligomers, the functional evidence from our transgenic *C. elegans* models further establishes this link. It is well-documented that the Y<sub>125</sub>EMPS<sub>129</sub> motif in  $\alpha$ -synuclein is required for the stabilization of  $\alpha$ -synuclein oligomers by dopamine *in vitro*. Mutation or deletion of this motif restores the ability of  $\alpha$ -synuclein to fibrillize in the presence of dopamine<sup>25</sup>, and the increase in oligomeric species in SH-SY5Y cells with elevated dopamine is prevented by expression of  $\alpha$ -synuclein that lacks this region<sup>27</sup>. Worms expressing A53T  $\alpha$ -synuclein specifically mutated in the Y<sub>125</sub>EMPS<sub>129</sub> domain were entirely resistant to the neurotoxic effects of increasing dopamine levels. Thus, preventing the interaction of dopamine and  $\alpha$ -synuclein and thereby inhibiting its effects on  $\alpha$ -synuclein oligomers is neuroprotective. Although we were not able to biochemically characterize  $\alpha$ -synuclein oligomer species in these worms as a result of expression in only eight cells in the entire animal, our findings nevertheless support a key role of dopamine in neurodegeneration, specifically through its influence on  $\alpha$ -synuclein.

Collectively, our findings underscore the potential critical importance of the interaction of dopamine and  $\alpha$ -synuclein in driving disease. In PD, dopaminergic terminals are thought to degenerate before cell bodies<sup>50</sup>, suggesting that the disease may arise at the synapse.

Increasing dopamine levels in A53T mice recapitulated the substantial loss of terminals that precedes overt nigral cell death, offering a new model of disease progression in PD. These mice also underwent an eventual decline in dopamine levels and developed an associated motor deficit, mimicking the depletion of striatal dopamine and the resulting hypokinesia that occurs in PD. Our findings also demonstrate that dopamine modifies  $\alpha$ -synuclein aggregation *in vivo*, resulting in oligomer conformations that are biochemically and structurally similar to neurotoxic oligomers induced by dopamine *in vitro*. Finally, we were able to rescue dopaminergic neurons from dopamine toxicity by specifically inhibiting its interaction with  $\alpha$ -synuclein in *C. elegans*. Dopamine-modified  $\alpha$ -synuclein species may mediate neurodegeneration by disrupting cellular membranes, as previously proposed for  $\alpha$ -synuclein oligomers<sup>49</sup>. Moreover, damage to synaptic vesicle membranes could lead to dopamine leakage and further induction of pathogenic  $\alpha$ -synuclein species.

## METHODS

Methods, including statements of data availability and any associated accession codes and references, are available in the [online version of the paper](#).

*Note: Any Supplementary Information and Source Data files are available in the online version of the paper.*

## ACKNOWLEDGMENTS

We thank T. Clarke and T. Pierson from the Wolfe lab for technical assistance with animals and for helpful advice on vector production. We thank H. Bennett from the Kalb lab for initial work on the dopamine neuron degeneration assay in *C. elegans* and input on worm breeding. We thank L. Spruce, H. Fazelina and S. Seeholzer from the Children's Hospital of Philadelphia Proteomic Core facility for mass spectrometry. We thank V. Lee (University of Pennsylvania) and G. Miller (Emory University) for generously providing  $\alpha$ -synuclein and VMAT2 antibodies, respectively, and S. Przedborski (Columbia University) for the use of stereology equipment and helpful feedback on the manuscript. Finally, we thank R. Lightfoot and members of the Ischiropoulos lab for productive discussions and technical support. This work was supported by grants from the US National Institutes of Health: AG013966 (H.I.), NS038690 (J.H.W.) and NS087077 and NS052325 (R.G.K.). D.E.M. was supported by the US National Institutes of Health Ruth L. Kirschstein National Research Service Award Individual Predoctoral Fellowship NS087779. The content of this work is solely the responsibility of the authors and does not necessarily represent the official views of the National Institutes of Health.

## AUTHOR CONTRIBUTIONS

D.E.M., E.T., J.R.M., R.G.K. and H.I. conceived and designed the experiments. D.E.M., E.T., H.K., N.S.G., M.J.D., S.D., P.G., J.L.G. and V.X.T. performed the experiments and analyzed the data. D.E.M. wrote the paper, with important contributions from J.R.M., E.T., J.H.W., R.G.K., K.A.C., G.A.C. and H.I.

## COMPETING FINANCIAL INTERESTS

The authors declare no competing financial interests.

Reprints and permissions information is available online at <http://www.nature.com/reprints/index.html>. Publisher's note: Springer Nature remains neutral with regard to jurisdictional claims in published maps and institutional affiliations.

1. Ehringer, H. & Hornykiewicz, O. Verteilung von noradrenalin und dopamin (3-hydroxytyramin) im gehirn des menschen und ihr verhalten bei erkrankungen des extrapyramidalen systems. [Distribution of noradrenaline and dopamine (3-hydroxytyramine) in the human brain and their behavior in diseases of the extrapyramidal system]. *Klin. Wochenschr.* **38**, 1236–1239 (1960).
2. Graham, D.G. Oxidative pathways for catecholamines in the genesis of neuromelanin and cytotoxic quinones. *Mol. Pharmacol.* **14**, 633–643 (1978).
3. Jenner, P. & Olanow, C.W. Oxidative stress and the pathogenesis of Parkinson's disease. *Neurology* **47** Suppl 3: S161–S170 (1996).
4. Dexter, D.T. *et al.* Basal lipid peroxidation in substantia nigra is increased in Parkinson's disease. *J. Neurochem.* **52**, 381–389 (1989).
5. Zhang, J. *et al.* Parkinson's disease is associated with oxidative damage to cytoplasmic DNA and RNA in substantia nigra neurons. *Am. J. Pathol.* **154**, 1423–1429 (1999).
6. Giasson, B.I. *et al.* Oxidative damage linked to neurodegeneration by selective alpha-synuclein nitration in synucleinopathy lesions. *Science* **290**, 985–989 (2000).



7. Hastings, T.G., Lewis, D.A. & Zigmond, M.J. Role of oxidation in the neurotoxic effects of intrastratial dopamine injections. *Proc. Natl. Acad. Sci. USA* **93**, 1956–1961 (1996).
8. Colebrooke, R.E. *et al.* Age-related decline in striatal dopamine content and motor performance occurs in the absence of nigral cell loss in a genetic mouse model of Parkinson's disease. *Eur. J. Neurosci.* **24**, 2622–2630 (2006).
9. Caudle, W.M. *et al.* Reduced vesicular storage of dopamine causes progressive nigrostriatal neurodegeneration. *J. Neurosci.* **27**, 8138–8148 (2007).
10. Polymeropoulos, M.H. *et al.* Mutation in the alpha-synuclein gene identified in families with Parkinson's disease. *Science* **276**, 2045–2047 (1997).
11. Krüger, R. *et al.* Ala30Pro mutation in the gene encoding alpha-synuclein in Parkinson's disease. *Nat. Genet.* **18**, 106–108 (1998).
12. Singleton, A.B. *et al.* alpha-Synuclein locus triplication causes Parkinson's disease. *Science* **302**, 841 (2003).
13. Chartier-Harlin, M.-C. *et al.* Alpha-synuclein locus duplication as a cause of familial Parkinson's disease. *Lancet* **364**, 1167–1169 (2004).
14. Zarranz, J.J. *et al.* The new mutation, E46K, of alpha-synuclein causes Parkinson and Lewy body dementia. *Ann. Neurol.* **55**, 164–173 (2004).
15. Proukakis, C. *et al.* A novel  $\alpha$ -synuclein missense mutation in Parkinson disease. *Neurology* **80**, 1062–1064 (2013).
16. Lesage, S. *et al.* French Parkinson's Disease Genetics Study Group. G51D  $\alpha$ -synuclein mutation causes a novel parkinsonian-pyramidal syndrome. *Ann. Neurol.* **73**, 459–471 (2013).
17. Pasanen, P. *et al.* Novel  $\alpha$ -synuclein mutation A53E associated with atypical multiple system atrophy and Parkinson's disease-type pathology. *Neurobiol. Aging* **35**, 2180.e1–2180.e5 (2014).
18. Spillantini, M.G. *et al.* Alpha-synuclein in Lewy bodies. *Nature* **388**, 839–840 (1997).
19. Baba, M. *et al.* Aggregation of alpha-synuclein in Lewy bodies of sporadic Parkinson's disease and dementia with Lewy bodies. *Am. J. Pathol.* **152**, 879–884 (1998).
20. Iwai, A. *et al.* The precursor protein of non-A beta component of Alzheimer's disease amyloid is a presynaptic protein of the central nervous system. *Neuron* **14**, 467–475 (1995).
21. George, J.M., Jin, H., Woods, W.S. & Clayton, D.F. Characterization of a novel protein regulated during the critical period for song learning in the zebra finch. *Neuron* **15**, 361–372 (1995).
22. Abeliovich, A. *et al.* Mice lacking alpha-synuclein display functional deficits in the nigrostriatal dopamine system. *Neuron* **25**, 239–252 (2000).
23. Murphy, D.D., Rueter, S.M., Trojanowski, J.Q. & Lee, V.M. Synucleins are developmentally expressed, and alpha-synuclein regulates the size of the presynaptic vesicular pool in primary hippocampal neurons. *J. Neurosci.* **20**, 3214–3220 (2000).
24. Conway, K.A., Rochet, J.C., Bieganski, R.M. & Lansbury, P.T. Jr. Kinetic stabilization of the alpha-synuclein protofibril by a dopamine-alpha-synuclein adduct. *Science* **294**, 1346–1349 (2001).
25. Norris, E.H. *et al.* Reversible inhibition of alpha-synuclein fibrillization by dopaminochrome-mediated conformational alterations. *J. Biol. Chem.* **280**, 21212–21219 (2005).
26. Mazzulli, J.R. *et al.* Cytosolic catechols inhibit alpha-synuclein aggregation and facilitate the formation of intracellular soluble oligomeric intermediates. *J. Neurosci.* **26**, 10068–10078 (2006).
27. Mazzulli, J.R., Armakola, M., Dumoulin, M., Parastatidis, I. & Ischiropoulos, H. Cellular oligomerization of alpha-synuclein is determined by the interaction of oxidized catechols with a C-terminal sequence. *J. Biol. Chem.* **282**, 31621–31630 (2007).
28. Herrera, F.E. *et al.* Inhibition of alpha-synuclein fibrillization by dopamine is mediated by interactions with five C-terminal residues and with E83 in the NAC region. *PLoS One* **3**, e3394 (2008).
29. Martinez-Vicente, M. *et al.* Dopamine-modified alpha-synuclein blocks chaperone-mediated autophagy. *J. Clin. Invest.* **118**, 777–788 (2008).
30. Choi, B.K. *et al.* Large  $\alpha$ -synuclein oligomers inhibit neuronal SNARE-mediated vesicle docking. *Proc. Natl. Acad. Sci. USA* **110**, 4087–4092 (2013).
31. Nakashima, A. *et al.* The mutation of two amino acid residues in the N-terminus of tyrosine hydroxylase (TH) dramatically enhances the catalytic activity in neuroendocrine AtT-20 cells. *J. Neurochem.* **82**, 202–206 (2002).
32. Giasson, B.I. *et al.* Neuronal alpha-synucleinopathy with severe movement disorder in mice expressing A53T human alpha-synuclein. *Neuron* **34**, 521–533 (2002).
33. Tieu, K. *et al.* D-beta-hydroxybutyrate rescues mitochondrial respiration and mitigates features of Parkinson disease. *J. Clin. Invest.* **112**, 892–901 (2003).
34. Tsika, E. *et al.* Distinct region-specific alpha-synuclein oligomers in A53T transgenic mice: implications for neurodegeneration. *J. Neurosci.* **30**, 3409–3418 (2010).
35. Souza, J.M., Giasson, B.I., Chen, Q., Lee, V.M. & Ischiropoulos, H. Dityrosine cross-linking promotes formation of stable alpha-synuclein polymers. Implication of nitrate and oxidative stress in the pathogenesis of neurodegenerative synucleinopathies. *J. Biol. Chem.* **275**, 18344–18349 (2000).
36. Luk, K.C. *et al.* Pathological  $\alpha$ -synuclein transmission initiates Parkinson-like neurodegeneration in nontransgenic mice. *Science* **338**, 949–953 (2012).
37. Lakso, M. *et al.* Dopaminergic neuronal loss and motor deficits in *Caenorhabditis elegans* overexpressing human alpha-synuclein. *J. Neurochem.* **86**, 165–172 (2003).
38. Cao, S., Gelwix, C.C., Caldwell, K.A. & Caldwell, G.A. Torsin-mediated protection from cellular stress in the dopaminergic neurons of *Caenorhabditis elegans*. *J. Neurosci.* **25**, 3801–3812 (2005).
39. Karpinar, D.P. *et al.* Pre-fibrillar alpha-synuclein variants with impaired beta-structure increase neurotoxicity in Parkinson's disease models. *EMBO J.* **28**, 3256–3268 (2009).
40. Cao, P. *et al.* Alpha-synuclein disrupted dopamine homeostasis leads to dopaminergic neuron degeneration in *Caenorhabditis elegans*. *PLoS One* **5**, e9312 (2010).
41. Fahn, S. *et al.* Levodopa and the progression of Parkinson's disease. *N. Engl. J. Med.* **351**, 2498–2508 (2004).
42. Olanow, C.W. Levodopa: effect on cell death and the natural history of Parkinson's disease. *Mov. Disord.* **30**, 37–44 (2015).
43. Lohr, K.M. *et al.* Increased vesicular monoamine transporter enhances dopamine release and opposes Parkinson disease-related neurodegeneration in vivo. *Proc. Natl. Acad. Sci. USA* **111**, 9977–9982 (2014).
44. Rochet, J.C., Conway, K.A. & Lansbury, P.T. Jr. Inhibition of fibrillization and accumulation of prefibrillar oligomers in mixtures of human and mouse alpha-synuclein. *Biochemistry* **39**, 10619–10626 (2000).
45. Specht, C.G. & Schoepfer, R. Deletion of the alpha-synuclein locus in a subpopulation of C57BL/6J inbred mice. *BMC Neurosci.* **2**, 11 (2001).
46. Mosharov, E.V. *et al.* Interplay between cytosolic dopamine, calcium and alpha-synuclein causes selective death of substantia nigra neurons. *Neuron* **62**, 218–229 (2009).
47. Winner, B. *et al.* In vivo demonstration that alpha-synuclein oligomers are toxic. *Proc. Natl. Acad. Sci. USA* **108**, 4194–4199 (2011).
48. Xu, J. *et al.* Dopamine-dependent neurotoxicity of alpha-synuclein: a mechanism for selective neurodegeneration in Parkinson disease. *Nat. Med.* **8**, 600–606 (2002).
49. Danzer, K.M. *et al.* Different species of alpha-synuclein oligomers induce calcium influx and seeding. *J. Neurosci.* **27**, 9220–9232 (2007).
50. Cheng, H.-C., Ulane, C.M. & Burke, R.E. Clinical progression in Parkinson disease and the neurobiology of axons. *Ann. Neurol.* **67**, 715–725 (2010).

## ONLINE METHODS

**Animals.** The mice (*Mus musculus*) used in this study were homozygous for expression of human A53T  $\alpha$ -synuclein under the mouse PrP promoter (line M83). These mice undergo spinal cord degeneration at approximately 18 months of age in our colony, and the phenotype has been described previously<sup>32</sup>. Any animals showing symptoms of spinal cord degeneration, that is, hunched back, altered gait, or hindlimb paralysis, were excluded from the study. NonTg littermates were also used for experiments. No care was taken as to the sex of the animals. Mice were randomly assigned to the lentiviral vector injection groups and subsequent analyses, and the organization of experimental conditions was also random. Data collection and analyses were not performed blind to the conditions of the experiments except where otherwise indicated. All animal work was conducted according to National Institute of Health guide for the care and use of laboratory animals and in compliance with procedures approved by the Children's Hospital of Philadelphia Institutional Animal Care and Use Committee.

**Production of lentiviral vectors and determination of titer.** Generation of human tyrosine hydroxylase-1 with mutation of R<sub>37</sub>R<sub>38</sub> to E<sub>37</sub>E<sub>38</sub> (TH-RREE) has been previously described<sup>26</sup>. The coding sequence was removed from the pcDNA3.1 vector and was subcloned into the self-inactivating pTY-linker lentiviral expression vector at the *Pme*I site downstream of the CMV promoter. Generation of replication-deficient pseudotyped HIV-derived lentiviral vectors was achieved by transient co-transfection of HEK293T cells with the expression vector along with the vectors carrying the additional transcripts required for encapsulation, packaging and envelope proteins. 24 h after the cells were seeded into 150-mm dishes coated with poly-D-lysine they were transiently transfected with a mixture containing 550  $\mu$ g of the pTY-TH-RREE expression vector, 357.5  $\mu$ g of CMVD82 packaging vector, and 192.5  $\mu$ g of pVSV-G envelope vectors using the calcium phosphate transfection protocol. The culture medium was changed every day and the media containing the virus was collected 72 h post-transfection, filtered through 0.45  $\mu$ m membranes, and concentrated by ultracentrifugation at 50,000 g for 2 h at 4 °C. The viral pellet was subsequently re-suspended in 800  $\mu$ l of DMEM medium to make a concentrated viral stock. An empty vector control virus containing all elements except for the gene encoding TH-RREE (CtrlVect) was generated in parallel and both viruses were obtained from the University of Pennsylvania Vector Core.

To determine vector functionality and viral titer, SH-SY5Y human neuroblastoma cells (American Type Culture Collection) were plated in 24-well plates at  $5 \times 10^4$  cells/well in DMEM/F12 medium containing 10% heat-inactivated FBS, 100 U/ml penicillin, and 100  $\mu$ g/ml streptomycin. The cells were allowed to recover for 2 d and were then differentiated for 5 d with 20  $\mu$ M retinoic acid. The cells were infected with different dilutions of CtrlVect or TH-RREE lentivirus and viral titers were calculated by TH immunocytochemistry as described previously<sup>26</sup> for three independent cell plating/infection experiments.

**Stereotaxic injection of lentiviral vector into the SN.** A53T  $\alpha$ -synuclein transgenic mice or non-transgenic littermates received bilateral lentiviral vector injections at 10 months of age. The mice were placed into an anesthesia chamber connected to an isoflurane delivery system to induce anesthesia. The mice were then placed into a stereotaxic head holder, an anesthesia mask was fitted, and an incision was made in the skin. Small bilateral holes were drilled into the skull according to the coordinates for the SN in the mouse brain (anterior-posterior  $-3.3$  mm from bregma, mediolateral 1 mm) and a 30g Hamilton syringe was inserted slowly to 4 mm dorsoventral depth. 2  $\mu$ l of the viral concentrate ( $5 \times 10^7$  IU/ml) was injected into the SN at a rate of 0.25  $\mu$ l/min, and the needle was left in place for an additional 5 min before being slowly withdrawn, in order to minimize leakage of the injected fluid. The skin was sutured sterilely and the animals were monitored until they recovered from anesthesia.

**Motor function testing.** All behavioral tests were conducted 1 week before sacrifice. Mice were habituated to the testing room for 2 h before testing. To measure open field activity, the mice were singly housed and the cage was placed inside a laser monitoring device consisting of an open, rectangular frame containing sensors (Opto-M3 activity meter, Columbus Instruments). The number of infrared beam breaks was quantified over a 12-h period during the dark cycle from 6 p.m. to 6 a.m. using Multi Device Interface software version 1.3 (Columbus Instruments). For each animal, data was collected for up to 3 consecutive days and averaged. Food and water were available *ad libitum*.

To assess motor coordination and balance, mice were tested on the Rotarod (Ugo Basile, model 7650). The mice were acclimated to the apparatus with four training sessions of 5 min each at 4 rpm, followed by 5 min of rest in the home cage. Testing was performed 1 h later with two trials in which speed was accelerated from 4 to 40 rpm in 300 s. For each mouse, the latency to fall off the rotarod within this time period was recorded for the two trials and averaged.

**Immunohistochemistry and stereological cell counts.** For histological analysis, the mice were deeply anesthetized and perfused transcardially with saline followed by 4% paraformaldehyde (PFA) in 0.1 M phosphate buffer (pH 7.4). The brains were post-fixed overnight at 4 °C in 4% PFA and then cryoprotected in 30% sucrose solution for 2 d at 4 °C. The brains were submerged in dry ice-chilled isopentane for 30 s and then stored at  $-80$  °C until sectioning. On the day of sectioning, brains were mounted on chucks with OCT (Tissue-Tek) and the brainstem, SN and striatum were each sectioned using a cryostat (Leica, Jung Frigocut 2800N). Free-floating coronal sections of alternating 10- and 30- $\mu$ m thickness were collected from each region and stored at 4 °C in 0.1 M phosphate buffer containing 0.01% sodium azide.

The sections were quenched in 5% H<sub>2</sub>O<sub>2</sub> in methanol for 30 min, followed by antigen retrieval by boiling in citrate solution pH 6 for 10 min. The tissue was blocked for 1 h at 20–25 °C with 5% NGS, 3% BSA in PBS containing 0.1% Triton X-100, and then incubated overnight at 4 °C with primary antibody diluted in blocking buffer. Antibodies were used against VMAT2 (rabbit, 1:20,000, Covance Custom Immunology Services; courtesy of G. Miller, Emory University)<sup>43</sup>, TH (rabbit, 1:2,000, Calbiochem 657012)<sup>51</sup>, and Syn505 (mouse, 1:5,000, courtesy of V.M. Lee, University of Pennsylvania)<sup>32</sup>. Incubation with biotin-conjugated secondary antibodies was followed by avidin-biotin-peroxidase complex, each for 1 h at 20–25 °C (Vector Laboratories PK-6101, PK-6102)<sup>34</sup>, and visualization by 3,3'-diaminobenzidine (DAB) for 1 min (Vector Laboratories). In some cases, sections were counterstained with Cresyl Violet. The tissue was then mounted, dehydrated in an increasing alcohol series and cleared in xylenes, and coverslipped with Permount mounting medium. Slides were scanned by the Children's Hospital of Philadelphia Pathology Core facility and images were accessed using Aperio Imagescope software version 11.2 (Leica Biosystems). Quantification of VMAT2 staining intensity in the striatum was performed using Image J software version 1.48 (National Institutes of Health).

Unbiased stereological quantification of neurons in the SN was performed as described previously<sup>33</sup>. Briefly, 30- $\mu$ m sections spaced 90  $\mu$ m apart were selected in order to represent the full rostro-caudal axis of the SN. The sections were stained with Cresyl Violet and the Nissl-positive neurons were blindly counted using the optical fractionator method (StereoInvestigator version 11.02.1, MBF Bioscience).

**Catechol quantification by HPLC with electrochemical detection.** Striatal tissues were homogenized by sonication in ten volumes of 0.1 M perchloric acid containing 1  $\mu$ M 3,4-dihydroxybenzylamine as an internal standard. The samples were centrifuged at 16,000 g for 10 min at 4 °C and the supernatants were filtered through 0.22- $\mu$ m filters. 50  $\mu$ l of each sample was injected onto an Agilent 1100 series HPLC controlled by ChemStation software version 1.04 (Agilent). Catechols were resolved on a reverse-phase C18 Luna column (150  $\times$  4.6 mm, 5  $\mu$ m; Phenomenex) and detected using a Coularray detector (ESA Biosciences) as previously described<sup>26</sup>. Protein pellets were solubilized in 50 mM Tris pH 7.4 containing 2% SDS and protein concentration was determined using the BCA microassay kit (Pierce). Monoamine levels were normalized to protein concentration and expressed as femtomoles analyte per  $\mu$ g of protein.

**Sequential extraction and native SEC.** Striatal or SN tissue from individual mice was homogenized in ten volumes of lysis buffer: 1% Triton X-100 in 20 mM HEPES pH 7.4, 150 mM NaCl, 10% glycerol, 1 mM EGTA, and protease inhibitor cocktail (P2714, Sigma). The tissue was grinded with a mechanical homogenizer and centrifuged at 16,000 g for 10 min at 4 °C. The pellet was further extracted by sonication in 2% SDS, 50 mM Tris pH 7.4 with protease inhibitor cocktail, boiling at 95 °C for 10 min, and centrifugation at 16,000 g for 10 min. The resulting supernatant was designated the Triton-insoluble fraction. Protein concentration was determined using the BCA assay (Pierce).

For SEC, 500  $\mu$ g of Triton-soluble SN tissue in a total volume of 270  $\mu$ l was loaded onto a Superdex 200 HR10/30 column (GE Healthcare) connected to an

Agilent 1100 series HPLC system controlled by ChemStation software version 1.04 (Agilent). Mobile phase consisted of 25 mM HEPES and 150 mM NaCl, pH 7.25 and the flow rate was set to 0.3 ml/min. Fractions corresponding to 122–94, 94–81, 81–72, 72–65, 65–59, 59–54, 54–50, 50–45, 45–41, 41–38, 38–34, and 34–32 Å were each pooled and concentrated with 3,000 NMWL Ultracel Microcon filters (Millipore). Fractions 122–72, 65–41, and 38–32 were further combined to enhance the  $\alpha$ -synuclein signal on SDS-PAGE. The SEC column was calibrated using globular protein standards (GE Healthcare).

**Western blotting.** Proteins sequentially extracted or further fractionated by SEC were run on 10% or 12% SDS-PAGE gels and transferred to PVDF membranes. The membranes were blocked for 1 h at 20–25 °C in 5% (w/v) milk in 20 mM Tris pH 7.4, 150 mM NaCl and 0.1% Tween. Incubation with primary antibodies diluted in blocking buffer was overnight at 4 °C. Antibodies used against synaptic proteins were TH (rabbit, 1:4,000, Calbiochem 657012)<sup>52</sup>, DAT (rat, 1:1,000, Millipore MAB369)<sup>36</sup>, D1 receptor (rat, 1:1,000, Sigma D2944)<sup>36</sup>, DARPP-32 (rabbit, 1:1,000, Cell Signaling 23065)<sup>53</sup>. Antibodies directed against  $\alpha$ -synuclein were LB509 (mouse, 1:1,000)<sup>32,34</sup>, Syn505 (mouse, 1:1,000)<sup>54</sup>, and SNL-4 (rabbit, 1:1,000)<sup>55</sup>, all courtesy of V.M. Lee, University of Pennsylvania. Loading controls for Triton-soluble proteins were GAPDH (mouse, 1:10,000, Abcam ab8245)<sup>56</sup>, NSE (rabbit, 1:4,000, Abcam ab53025)<sup>57</sup>, and Actin (rabbit, 1:1,000, Sigma A2066)<sup>58</sup>. The loading control for Triton-insoluble proteins was Vimentin (mouse, 1:1,000, BD Pharmingen 550513)<sup>34</sup>. Membranes were incubated for 1 h at 20–25 °C with secondary antibodies conjugated to IRDye 680 or 800 (1:5,000, Rockland)<sup>34</sup> and then scanned using an Odyssey Infrared Imaging System (Li-Cor). Quantification of protein levels was performed using ImageStudio software version 4.0.21 (Li-Cor) and was normalized to loading control levels. For  $\alpha$ -synuclein oligomer bands, all individual immunobands >19 kD that were detected were quantified and the intensities summed, and the total was divided by the total NSE.

Near-infrared (nIRF) scanning of oxidized catechols was performed as described previously<sup>59</sup>. Briefly, before transfer the SDS-PAGE gels were scanned in the 700-nm channel at intensity 10 on an Odyssey Infrared Imaging System (Li-Cor).

**Immunoelectron microscopy of SEC fractions.** SEC fractions from SN tissue corresponding to low (41–65) and high (72–122) angstrom Stokes radii or dopamine-incubated recombinant  $\alpha$ -synuclein were applied to 300 mesh carbon-coated grids and blocked with 1% BSA in 20 mM Tris pH 7.4, 150 mM NaCl. The  $\alpha$ -synuclein oligomers were labeled with the Syn505 antibody against the N terminus or LB509 antibody against the C terminus, followed by 10 nm gold conjugated secondary (Electron Microscopy Sciences) as previously described<sup>25</sup>. Grids were negatively stained with 1% uranyl acetate and imaged at the University of Pennsylvania Electron Microscopy Resource Laboratory. Control samples were immunodepleted of  $\alpha$ -synuclein (see below) before grid preparation or had primary antibody omitted.

**In vitro aggregation and seeding assays.** Recombinant human wild-type  $\alpha$ -synuclein was expressed and purified as described previously<sup>34</sup>. Purified  $\alpha$ -synuclein was incubated at 6 mg/ml (415  $\mu$ M) with or without equimolar dopamine at 37 °C and shaking at 1,400 rpm for up to 6 d. At indicated time points, fibrillar content of the reaction mixture was assayed by the addition of Thioflavin T (Sigma) to a final concentration of 25  $\mu$ M. Fluorescence emission was measured at 482 nm during excitation at 450 nm. Sedimentation analysis was performed by centrifugation at 16,000 g for 10 min at 4 °C. The supernatants and pellets were boiled in SDS sample buffer at 95 °C for 10 min.  $\alpha$ -Synuclein aggregates were resolved by SDS-PAGE and the gels were stained with Coomassie Blue R-250. Circular dichroism spectra were obtained using a Jasco J-810 spectropolarimeter at the Children's Hospital of Philadelphia Protein Core facility. The protein was diluted to 20  $\mu$ M in 0.05 M KH<sub>2</sub>PO<sub>4</sub> pH 7.8. Spectra were corrected for baseline measurement of an equivalent volume of PBS diluted in KH<sub>2</sub>PO<sub>4</sub> buffer. The *n* value reported equals the number of independent aggregation assays.

Seeding assays were performed by incubating 5  $\mu$ g total protein from pooled oligomeric SEC fractions (41–122 Å) for each mouse with 425  $\mu$ g fresh recombinant  $\alpha$ -synuclein (300  $\mu$ M final concentration) at 37 °C and shaking at 1,400 rpm. Aliquots at indicated time points were analyzed by Thioflavin T. To immunodeplete  $\alpha$ -synuclein for control samples, pooled SEC fractions were incubated overnight at 4 °C with LB509 antibody at a 1:5 ratio of antibody to total  $\mu$ g protein.

Protein G-conjugated beads (Sigma) were equilibrated in 25 mM HEPES, 150 mM NaCl, pH 7.4 and incubated with the immunocomplexes for 1 h at 4 °C.  $\alpha$ -Synuclein oligomers were then pulled down by centrifugation at 2,000 g for 2 min, and the resulting supernatant was used for experiments.

**C. elegans models.**  $\alpha$ -Synuclein plasmids for microinjection into worms were generated using Gateway technology (Invitrogen). Plasmids containing sequences for human A53T  $\alpha$ -synuclein or A53T  $\alpha$ -synuclein with Y<sub>125</sub>EMPS<sub>129</sub> mutated to F<sub>125</sub>AAFA<sub>129</sub> [A53T(125–9m)] were generated previously<sup>27</sup>. The coding sequences were PCR-amplified with addition of flanking attB1 and attB2 sites, and the resulting fragments were used to generate Gateway entry vectors by BP reaction with pDONR221. LR reactions were then performed with each entry vector and the previously constructed pDEST-DAT-1 destination vector containing the *dat-1* promoter<sup>38</sup>. All primer sequences are available upon request.

Nematodes were maintained using well-established methods<sup>60</sup>. Constructs were injected into worms to create transgenic animals as previously described<sup>61</sup>. Strains UA287 (*baEx168 a,b,c* [*P<sub>dat-1</sub>::A53T  $\alpha$ -synuclein*, *P<sub>unc-54</sub>::tdTomato*]; *vtIs7* [*P<sub>dat-1</sub>::GFP*]) and UA288 (*baEx169 a,b,c* [*P<sub>dat-1</sub>::A53T(125–9m)  $\alpha$ -synuclein*, *P<sub>unc-54</sub>::tdTomato*]; *vtIs7* [*P<sub>dat-1</sub>::GFP*]) were generated by injecting a solution of 50 ng/ $\mu$ l of either *P<sub>dat-1</sub>::A53T  $\alpha$ -synuclein* or *P<sub>dat-1</sub>::A53T(125–9m)  $\alpha$ -synuclein* into strain BY250 (*vtIs7* [*P<sub>dat-1</sub>::GFP*]) with a phenotypic marker (*P<sub>unc-54</sub>::tdTomato*, 50 ng/ $\mu$ l, for body wall muscle expression). Three independent stable lines were created for each group (*a*, *b*, *c*). To analyze CAT-2 overexpression in these same backgrounds, we removed the *P<sub>dat-1</sub>::GFP* transgene from the UA287 and UA288 transgenic backgrounds by outcrossing to the N2 background. Then these two strains, which still contained the *P<sub>unc-54</sub>::tdTomato* phenotypic marker, were both crossed into UA57 (*baln4* [*P<sub>dat-1</sub>::CAT-2*, *P<sub>dat-1</sub>::GFP*]), generating UA296 (*baEx168 a,b,c* [*P<sub>dat-1</sub>::A53T  $\alpha$ -synuclein*, *P<sub>unc-54</sub>::tdTomato*]; *baln4* [*P<sub>dat-1</sub>::CAT-2*, *P<sub>dat-1</sub>::GFP*]) and UA297 (*baEx169 a,b,c* [*P<sub>dat-1</sub>::A53T(125–9m)  $\alpha$ -synuclein*, *P<sub>unc-54</sub>::tdTomato*]; *baln4* [*P<sub>dat-1</sub>::CAT-2*, *P<sub>dat-1</sub>::GFP*]).

For dopaminergic neurodegeneration analyses, transgenic hermaphroditic animals were scored as described previously<sup>62</sup>. Briefly, on the day of analysis, the six anterior dopaminergic neurons [four CEP (cephalic) and two ADE (anterior deirid)] were examined in 30 randomly selected worms that also express the *tdTomato* marker in the body wall muscle cells. Each animal was considered normal when there was a full complement of six anterior DA neurons. However, if a worm exhibited any degenerative phenotype, such as a missing dendritic process, cell body loss, or a blebbing neuronal process, it was scored as degenerating. Three independent transgenic worm lines were analyzed per genetic background and an average of the total percentage of worms with normal neurons was reported in the study.

For label-free quantification of  $\alpha$ -synuclein expression by mass spectrometry, protein from GFP and *tdTomato* positive day 1 adult nematodes was extracted in a buffer containing 50 mM Tris, pH 7.5 with 8 M urea and 2% SDS. 50  $\mu$ g of soluble protein underwent buffer exchange to PBS and concentrated using 10 kDa cutoff spin filters (Amicon). The concentrated protein was combined with 6 $\times$  loading buffer and run on a 10% NuPAGE gel with MES running buffer (Invitrogen). The gel was fixed and stained using Novex Colloidal Blue staining kit (Invitrogen). Purified recombinant  $\alpha$ -synuclein was used as a marker for sample bands of interest. Sample bands of interest with apparent molecular weight of 14 kDa were excised from the gel and digested with trypsin overnight. Trypsin digests were then analyzed by LC-MS/MS on a hybrid LTQ Orbitrap Elite mass spectrometer (ThermoFisher) coupled with a nanoLC Ultra (Eksigent). The mass spectrometer was set for parallel reaction monitoring for human  $\alpha$ -synuclein sequence with the A53T mutation.

**Primary neuronal cultures.** Hippocampal neurons were provided by the University of Pennsylvania Neuron Culture Service Center. After dissection from C57BL/6 mouse embryos at day 18–19, cells were mechanically dissociated, trypsinized, and seeded at 100,000 cells per well into 24-well plates freshly coated with 50  $\mu$ g/ml poly-D-lysine (Sigma). After plating, neurons were cultured for 2 h in culture media containing 5% heat-inactivated FBS, 1% Glutamax, 2% B-27 supplement, 100 U/ml penicillin, 100  $\mu$ g/ml streptomycin in Neurobasal media (all from Invitrogen). After 2 h, the media was changed to culture media without FBS to discourage survival of glial cells. Twice per week, half of the media was replaced with fresh culture media.



Following 1 week in culture, neurons were treated with dopamine-incubated  $\alpha$ -synuclein (from day 4–6 of *in vitro* aggregation) at a final concentration of 1  $\mu$ M. Control conditions were equivalent doses of PBS, monomeric  $\alpha$ -synuclein, or dopamine that had been incubated in parallel under aggregation conditions but without  $\alpha$ -synuclein. 2 weeks post-treatment, cell viability was assayed using calcein AM (Sigma) and propidium iodide (PI) (Sigma) incubated for 20 min at 20–25 °C at final concentrations of 3  $\mu$ M in PBS. Fluorescence images were obtained using MetaMorph software version 7.7 (Molecular Devices) and an inverted Olympus IX70 microscope equipped with an IX-FLA fluorescence observation attachment (Olympus Optical). For quantification of viable cells (calcein positive and PI negative), at least ten random fields of view were blindly counted per treatment condition and averaged to obtain one replicate value. Independent culture experiments performed with separate plating/treatments were considered independent replicates and were reported as the *n* value.

To image human  $\alpha$ -synuclein in treated neurons, cells were labeled in a two-stage protocol as previously described<sup>63</sup>. 2 weeks following treatment, cells were live-incubated in media containing Syn204 antibody (mouse IgG2a, 1:500) for 1 h at 4 °C to label extracellular  $\alpha$ -synuclein. The cells were then fixed with 4% PFA for 20 min at 20–25 °C, and permeabilized with 0.1% Triton X-100 in 5% NGS, 3% BSA in PBS for 1 h at 20–25 °C. Cells were incubated with LB509 (mouse IgG1, 1:500) overnight at 4 °C to label both extracellular and intracellular  $\alpha$ -synuclein. Secondary antibodies conjugated to Alexa Fluor (anti-mouse IgG1 488, 1:500, Thermo Fisher A21121; anti-mouse IgG2a 594, 1:500, Thermo Fisher A-21135) were incubated for 1 h at 20–25 °C. The staining was imaged by laser-scanning confocal microscopy (Olympus Fluoview) and the *n* value equals the number of independent culture experiments.

**Statistics.** All statistical analysis was done using Prism 6 software (GraphPad). Two-tailed unpaired Student's *t* test was used for all comparisons between two groups. For comparisons with multiple groups, one-way ANOVA using Tukey's *post hoc* correction for multiple comparisons. Specifically for Thioflavin T assays with multiple groups measured over time, repeated-measures two-way ANOVA with Tukey's or Bonferroni's correction for multiple comparisons was used. No statistical methods were used to pre-determine sample sizes but our sample sizes are similar to those reported previously<sup>34,36</sup>. All experiments were performed

at least twice, with measurements from the same samples treated as technical replicates. In the case of representative images, several images per sample were obtained. Readers are referred to the **Life Sciences Reporting Summary** available online for additional information.

**Data Availability Statement.** The data that support the findings of this study are available from the corresponding author upon reasonable request.

51. Brichta, L. *et al.* Identification of neurodegenerative factors using translational-regulatory network analysis. *Nat. Neurosci.* **18**, 1325–1333 (2015).
52. Khasnavis, S., Ghosh, A., Roy, A. & Pahan, K. Castration induces Parkinson disease pathologies in young male mice via inducible nitric-oxide synthase. *J. Biol. Chem.* **288**, 20843–20855 (2013).
53. Qian, Y., Forssberg, H. & Diaz Heijtz, R. Motor skill learning is associated with phase-dependent modifications in the striatal cAMP/PKA/DARPP-32 signaling pathway in rodents. *PLoS One* **10**, e0140974 (2015).
54. Waxman, E.A., Duda, J.E. & Giasson, B.I. Characterization of antibodies that selectively detect alpha-synuclein in pathological inclusions. *Acta Neuropathol.* **116**, 37–46 (2008).
55. Luk, K.C. *et al.* Intracerebral inoculation of pathological  $\alpha$ -synuclein initiates a rapidly progressive neurodegenerative  $\alpha$ -synucleinopathy in mice. *J. Exp. Med.* **209**, 975–986 (2012).
56. Eales, K.L. *et al.* The MK2/3 cascade regulates AMPAR trafficking and cognitive flexibility. *Nat. Commun.* **5**, 4701 (2014).
57. Sun, Y. *et al.* The expression and significance of neuronal iconic proteins in podocytes. *PLoS One* **9**, e93999 (2014).
58. Sarkar, S., Davies, J.E., Huang, Z., Tunnacliffe, A. & Rubinsztein, D.C. Trehalose, a novel mTOR-independent autophagy enhancer, accelerates the clearance of mutant huntingtin and alpha-synuclein. *J. Biol. Chem.* **282**, 5641–5652 (2007).
59. Mazzulli, J.R., Burbulla, L.F., Krainc, D. & Ischiropoulos, H. Detection of free and protein-bound ortho-quinones by near-infrared fluorescence. *Anal. Chem.* **88**, 2399–2405 (2016).
60. Brenner, S. The genetics of *Caenorhabditis elegans*. *Genetics* **77**, 71–94 (1974).
61. Berkowitz, L.A., Knight, A.L., Caldwell, G.A. & Caldwell, K.A. Generation of stable transgenic *C. elegans* using microinjection. *J. Vis. Exp.* **18**, 833 (2008).
62. Hamamichi, S. *et al.* Hypothesis-based RNAi screening identifies neuroprotective genes in a Parkinson's disease model. *Proc. Natl. Acad. Sci. USA* **105**, 728–733 (2008).
63. Volpicelli-Daley, L.A. *et al.* Exogenous  $\alpha$ -synuclein fibrils induce Lewy body pathology leading to synaptic dysfunction and neuron death. *Neuron* **72**, 57–71 (2011).

## Life Sciences Reporting Summary

Nature Research wishes to improve the reproducibility of the work that we publish. This form is intended for publication with all accepted life science papers and provides structure for consistency and transparency in reporting. Every life science submission will use this form; some list items might not apply to an individual manuscript, but all fields must be completed for clarity.

For further information on the points included in this form, see [Reporting Life Sciences Research](#). For further information on Nature Research policies, including our [data availability policy](#), see [Authors & Referees](#) and the [Editorial Policy Checklist](#).

## ► Experimental design

## 1. Sample size

Describe how sample size was determined.

No statistical methods were used to pre-determine sample sizes but our sample sizes are similar to those reported in previous publications (ref. 34, 36, 62).

## 2. Data exclusions

Describe any data exclusions.

The mice used in this study undergo spinal cord degeneration at approximately 18 months of age in our colony, and the phenotype has been described previously (ref. 32). Any animals showing symptoms of spinal cord degeneration, i.e. hunched back, altered gait, or hindlimb paralysis, were excluded from the study.

## 3. Replication

Describe whether the experimental findings were reliably reproduced.

All attempts at replication were successful.

## 4. Randomization

Describe how samples/organisms/participants were allocated into experimental groups.

Mice were randomly assigned to the lentiviral vector injection groups and subsequent analyses. Transgenic worms were randomly chosen for analysis.

## 5. Blinding

Describe whether the investigators were blinded to group allocation during data collection and/or analysis.

Data collection and analyses were not performed blind to the conditions of the experiments except for stereological quantification of neurons, and counting of cells in culture.

Note: all studies involving animals and/or human research participants must disclose whether blinding and randomization were used.

## 6. Statistical parameters

For all figures and tables that use statistical methods, confirm that the following items are present in relevant figure legends (or in the Methods section if additional space is needed).

n/a Confirmed

- ☐ ☒ The exact sample size (*n*) for each experimental group/condition, given as a discrete number and unit of measurement (animals, litters, cultures, etc.)
- ☐ ☒ A description of how samples were collected, noting whether measurements were taken from distinct samples or whether the same sample was measured repeatedly
- ☐ ☒ A statement indicating how many times each experiment was replicated
- ☐ ☒ The statistical test(s) used and whether they are one- or two-sided (note: only common tests should be described solely by name; more complex techniques should be described in the Methods section)
- ☐ ☒ A description of any assumptions or corrections, such as an adjustment for multiple comparisons
- ☐ ☒ The test results (e.g. *P* values) given as exact values whenever possible and with confidence intervals noted
- ☐ ☒ A clear description of statistics including central tendency (e.g. median, mean) and variation (e.g. standard deviation, interquartile range)
- ☐ ☒ Clearly defined error bars

See the web collection on [statistics for biologists](#) for further resources and guidance.

## ► Software

Policy information about [availability of computer code](#)

### 7. Software

Describe the software used to analyze the data in this study.

All statistical analysis was done using Prism 6 (GraphPad). Open field testing used Multi Device Interface version 1.3 (Columbus Instruments). Images of tissue staining were accessed using Aperio Imagescope version 11.2 (Leica Biosystems) and quantification of staining was performed using Image J version 1.48 (National Institutes of Health). Stereological cell counts were done using StereoInvestigator version 11.02.1 (MBF Bioscience). HPLC analyses were done using ChemStation version 1.04 (Agilent), and catechol quantification additionally used ESA CoulArray version 3.10. Fluorescence images were obtained using MetaMorph version 7.7 (Molecular Devices). Western blot band intensities were quantified using ImageStudio software version 4.0.21 (Li-Cor).

For manuscripts utilizing custom algorithms or software that are central to the paper but not yet described in the published literature, software must be made available to editors and reviewers upon request. We strongly encourage code deposition in a community repository (e.g. GitHub). *Nature Methods* [guidance for providing algorithms and software for publication](#) provides further information on this topic.

## ► Materials and reagents

Policy information about [availability of materials](#)

### 8. Materials availability

Indicate whether there are restrictions on availability of unique materials or if these materials are only available for distribution by a for-profit company.

There are no restrictions on availability of unique materials, such as TH-RREE and CtrlVect plasmids.

### 9. Antibodies

Describe the antibodies used and how they were validated for use in the system under study (i.e. assay and species).

The following antibodies were used: VMAT2 (Covance Custom Immunology Services, ref. 43), TH (Calbiochem, ref. 51, 52), Syn505 (ref. 32, 54), DAT (Millipore, ref. 36), D1R (Sigma, ref. 36), DARPP-32 (Cell Signaling, ref. 53), LB509 (ref. 32, 34), SNL-4 (ref. 55), GAPDH (Abcam, ref. 56), NSE (Abcam, ref. 57), Actin (Sigma, ref. 58), Vimentin (BD Pharmingen, ref. 34), Syn204 (ref. 63).

### 10. Eukaryotic cell lines

a. State the source of each eukaryotic cell line used.

SH-SY5Y human neuroblastoma cells were obtained from American Type Culture Collection.

b. Describe the method of cell line authentication used.

No cell line authentication was performed.

c. Report whether the cell lines were tested for mycoplasma contamination.

No test for mycoplasma contamination was performed.

d. If any of the cell lines used are listed in the database of commonly misidentified cell lines maintained by [ICLAC](#), provide a scientific rationale for their use.

No commonly misidentified cell lines were used.

## ► Animals and human research participants

Policy information about [studies involving animals](#); when reporting animal research, follow the [ARRIVE guidelines](#)

### 11. Description of research animals

Provide details on animals and/or animal-derived materials used in the study.

The mice (*Mus musculus*) used in this study were homozygous for expression of human A53T  $\alpha$ -synuclein under the mouse PrP promoter (line M83) (ref. 32), and non-transgenic littermates. No care was taken as to the sex of the animals. Mice were 10 months old at viral injection and either 12.5 or 15 months old at analysis. Four transgenic *C. elegans* strains were generated and hermaphrodites were analyzed at 3, 5, and 6 days post-hatching. Primary neuronal cultures were derived from C57BL/6 mouse embryos at day 18-19.

Policy information about [studies involving human research participants](#)

### 12. Description of human research participants

Describe the covariate-relevant population characteristics of the human research participants.

The study did not involve human research participants.